




Seismic vulnerability and loss assessment of an isolated simply-supported highway bridge retrofitted with optimized superelastic shape memory alloy cable restrainers

Shuai Li^{1,2} · Farshad Hedayati Dezfuli² · Jing-quan Wang¹ · M. Shahria Alam² 

Received: 8 October 2019 / Accepted: 24 February 2020 / Published online: 3 March 2020
© Springer Nature B.V. 2020

Abstract

Restrainers, being of relatively low cost and easy to install, are often used to prevent unseating of bridge spans. The potential of using superelastic shape memory alloy (SMA) restrainers in preventing such failure has been discussed in the literature; however, the impact of such smart restrainers with optimized configurations in reducing the failure probability of bridge components and system as well as the long-term economic losses given different earthquake scenarios has not been investigated yet. This study presents a probabilistic seismic fragility and long-term performance assessment on isolated multi-span simply-supported bridges retrofitted with optimized SMA restrainers. First, SMA restrainers are designed following the displacement-based approach and their configuration is optimized. Then, seismic fragility assessment is conducted for the bridge retrofitted with optimized SMA restrainers and compared with those of the original bridge and the bridges with elastic restrainers (steel and CFRP). Finally, long-term seismic loss (both direct and indirect) are evaluated to assess the performance of the retrofitted bridges in a life-cycle context. Results showed that among three considered restrainers, SMA restrainers make the bridge less fragile and help the system lower long-term seismic loss. The design event (DE, 2475-year return period) specified in Canadian Highway Bridge Design Code (CHBDC, CSA S6-14 2014) may underestimate the long-term seismic losses of the highway bridges. Under DE, the damage probability of the bridge retrofitted with optimized SMA restrainers experiencing collapse damage is only 0.7%. Under the same situation, its expected long-term loss is approximate 17.6% of that with respect to the unretrofitted bridge.

Keywords Cable restrainer · Highway bridge · Lead rubber bearing · Seismic fragility · Damage states

List of symbols

a and b Regression coefficient
 ADT Average daily traffic to detour

✉ Jing-quan Wang
wangjingquan@seu.edu.cn

✉ M. Shahria Alam
shahria.alam@ubc.ca

| | |
|-----------------|---|
| $ADTE$ | Average daily traffic remaining on the damaged link |
| A_r | Design area of the restrainer |
| c_1 | Damping coefficient of the pier |
| c_{AW} | Average wages for car drivers per hour |
| c_{ATC} | Average wages for truck drivers per hour |
| c_b | Equivalent viscous damping of bearing |
| c_{goods} | Time value of goods transported in a cargo |
| c_r | Equivalent viscous damping of the restrainer |
| c_{reb} | Rebuilding cost per square meter |
| $c_{run,car}$ | Average costs for running cars per kilometer |
| $c_{run,truck}$ | Average costs for running trucks per kilometer |
| $C_{DS,i}$ | Consequences at a certain damage state, i |
| $C_{REP,i}$ | Repair cost of a bridge at damage state i |
| C_{RUN} | Running costs |
| C_{TL} | Monetary time lost for users and goods traveling |
| d_i | Duration of the detour |
| D_l | Detour distance |
| EDP | Engineering demand parameter |
| f_a | Stress of restrainer at allowable displacement, Δ_a |
| F_b | Restoring force of bearing at allowable displacement, Δ_a |
| F_r | Required strength of restrainer |
| $F_{inertia}$ | Inertia force of girder |
| h_r | Vertical distance between two anchored ends of restrainer |
| IM | Intensity measure |
| k_1 | Stiffness of pier |
| k_b | Effective stiffness of isolation bearing |
| k_r | Effective stiffness of restrainer |
| l | Route segment containing bridge |
| L | Length of bridge |
| $L(t_k)$ | Expected annual hazard loss at time t_k |
| LCL | Total life-cycle hazard loss |
| L_i | Loss of bridge at damage state i |
| L_{r0} | Design length of restrainer at initial condition |
| L_{r1} | Length of restrainer at design target displacement condition |
| m_1 | Mass of bridge pier |
| m_2 | Mass of bridge girder |
| n_b | Number of isolation bearings at each pier or abutment location |
| N | Total number of simulation cases |
| $N(t_{int})$ | Number of earthquakes that occur during the time interval |
| o_{car} | Average vehicle occupancies for cars |
| o_{truck} | Average vehicle occupancies for trucks |
| $P[F_i]$ | Failure probabilities of i th component |
| $P_{DS,i PGA}$ | Conditional probability of a bridge at damage state i for a given PGA |
| P_s | Failure probabilities of system |
| R_{rcr} | Repair cost ratio at damage state i |
| S | Average detour speed |
| S_0 | Average speed on intact link |
| $SA(T, \xi_0)$ | Design response spectra ordinate for period T and damping ratio ξ_0 |
| S_c | Median estimate of capacity |

| | |
|----------------------------|--|
| S_D | Average speed on damaged link |
| t_{int} | Investigated time interval |
| T_0 | Ratio of average daily truck traffic |
| u_1 | Displacement of bridge pier |
| u_2 | Displacement of bridge girder |
| \ddot{u}_g | Ground acceleration |
| W | Width of bridge |
| Δ_a | Allowable relative displacement between bridge girder and pier |
| Δ_d | Design target displacement of restrainer |
| Δ_{rd} | Relative displacement between girder and pier |
| Δ_s | Slack of restrainer |
| θ_0 | Horizontal angle of restrainer at initial condition |
| θ_1 | Horizontal angle of restrainer at design target displacement condition |
| Φ | Cumulative distribution function of standard normal distribution |
| α | Normalized elongation ratio of restrainer |
| β_c | Logarithmic standard deviation of capacity |
| β_{DIIM} | Standard deviation of demand |
| γ | Shear strain of isolation bearing |
| ε_{max} | Maximum applied strain of SMA |
| λ | Median value of IM |
| ξ | Standard deviation of IM |
| μ_d | Displacement ductility of pier |
| τ | Monetary discount rate |

1 Introduction

Simply supported highway bridges are widely found in the transportation network. For example, more than 105,300 simply supported bridges make up more than 60% of the total number of bridges (163,433) in the central and southeastern United States alone (Nielson 2005). There are more than 1700 simply supported bridges making up more than 66% of the total number of highway bridges (2555) in British Columbia, Canada (Siddiquee and Alam 2017). However, damage observations have revealed that such bridges are highly vulnerable during previous seismic events (Kawashima et al. 2009; Naeim and Kelly 1999). For instance, in the 2008 Wenchuan earthquake in China, more than 27 multi-span simply-supported (MSSS) bridges experienced severe damage or complete collapse (Chen 2012). Typical damages of these bridges included sliding of the bearing, pier damage, shear key failure, and unseating of bridge spans (Xiang and Li 2017). These damage examples have raised public concerns about the seismic safety of MSSS bridges.

Different types of control strategies have been developed to prevent bridge failures during seismic events. Isolation bearings as one of the most popular techniques, such as natural rubber bearing, lead rubber bearing, high damping rubber bearing, are being widely adopted for highway bridges around the world, especially in Japan and the USA (Alam et al. 2012). Their efficiency in suppressing the transmission of the input earthquake energy has been proved during recent earthquakes (Xie and Zhang 2016), analytical studies (Liao et al. 2004; Shen et al. 2004; Zhang and Huo 2009; Ozbulut and Hurlbaas 2010; Li et al. 2018a, b), and experimental researches (Hwang et al. 2002; Xiang et al. 2018). However, considering the high flexibility of isolation bearings, such devices may experience large

deformation under strong earthquake excitations, especially near-fault ground motions, and as a result, some critical problems may arise, e.g. the instability of the isolation bearings and unseating of the deck (Ozbulut and Hurlbaeus 2011; Li et al. 2018a, b). Since the unseating of bridge spans is one of the main causes of collapse for MSSS bridges, isolation devices may not be always beneficial for such bridges.

As suggested by several seismic design guidelines, such as AASHTO LRFD (AASHTO 2012), Caltrans BDA (Caltrans 2013), Eurocode 8 (Eurocode 2005), Canadian Highway Bridge Design Code (CSA S6-14 2014), restraining devices can be chosen to retrofit the highway bridges to prevent the unseating problems of bridge spans. In the last 20 years, different types of restraining devices (e.g. restrainer or damper) have been developed to limit the displacement (Saiidi et al. 2001; DesRoches et al. 2003; Julian et al. 2007; Andrawes and DesRoches 2007b; Johnson et al. 2008; Padgett and DesRoches 2008; Markogiannaki and Tegos 2014; Aryan and Ghassemieh 2015; Joghataie and Pahlavan 2015, 2017; Wang et al. 2019a, b). The efficiency of restrainers has been verified in the literature; however, restrainer failures were still observed during the 1989 Loma Prieta, 1994 Northridge, and 1995 Kobe earthquakes (Schiff 1995; Andrawes and DesRoches 2007a) due to the inherent flaws in the design of the restrainers. Current design guidelines ignore the dynamic interactions between the superstructure and substructure. More recently, the present authors have proposed a new restrainer design procedure for isolated highway bridges (Li et al. 2018a). The failure probabilities of unseating were analyzed to verify the efficiency of the proposed method. The influence of restrainers on the seismic performance of critical structural components (such as bearings and piers) and the overall bridge system has not been thoroughly discussed. Another important point is that the restrainers used in Li et al. (2018a) were not installed in an optimized configuration. In a recent paper, the same authors used a fractional factorial design method to identify the optimized configuration of SMA restrainers in the bridge (Wang et al. 2019a, b). While the previous studies (Li et al. 2018a; Wang et al. 2019b) proved the potential of using SMA restrainers in bridges and proposed some design guidelines, adoption of these guidelines and successful implementation require a complete performance-based evaluation of this structural system in light of performance-based earthquake engineering (PBEE). However, to the best of authors' knowledge, no study has been directed towards understanding the performance of such a retrofitted bridge with optimized restrainers and how restrainers in an optimized configuration may impact the overall safety of the bridge under seismic events.

Numerous experimental and numerical studies have explored the efficiency of steel, FRP, and SMA cable restrainers in limiting the displacement of bridge systems in seismic regions (Saiidi et al. 1996, 2001, 2006; Andrawes and DesRoches 2005, 2007a, b; Padgett et al. 2010; Guo et al. 2012; Joghataie and Pahlavan 2017; Shrestha et al. 2018). Due to the low price, steel cables and high-strength steel bars are the primary forms of seismic restrainers to retrofit the bridges (Saiidi et al. 2006). Considering the easy installation and fabrication, FRP with high tensile strength and versatility is a potential candidate for seismic restrainers. The effectiveness of FRP restrainers in limiting relative hinge movement has been experimentally verified by Saiidi et al. (2006). However, both steel and FRP restrainers are generally designed to remain elastic and cannot dissipate any energy during earthquakes, and consequently, they may transfer larger earthquake force to the bridge piers. For addressing the shortcomings of traditional restrainers, shape memory alloy (SMA) cables/rods with superior energy dissipation and self-centering capacity have been proposed as restrainers by several researchers (DesRoche and Delemont 2002; Andrawes and DesRoches 2007a, b; Ozbulut and Hurlbaeus 2011; Bhuiyan and Alam 2012; Alam et al. 2012; Li et al. 2018a; Wang et al. 2019b). However, decision-makers

are yet to recognize the long-term performance benefit of the bridges retrofitted with such smart materials as they incur a higher initial cost. Most of the previous studies conducted the seismic performance assessment of the bridge retrofitted with SMA restrainers compared to a conventional bridge. Some studies extended the analysis to determine the initial cost of construction of such a bridge system. However, these two parameters alone would not necessarily give a holistic image regarding the overall performance of the structure. The performance benefit associated with the bridge retrofitted with SMA restrainer has not been well recognized by the decision-makers and the corresponding life-cycle loss has not been emphasized in the decision-making process. Hence, the application of SMA in civil infrastructures is still limited. In this regard, the long-term performance-based engineering (PBE) is necessary to be conducted to aid the decision-making of government and promote the application of novel materials in civil engineering.

The objective of this study is to explore the impact of SMA restrainers with the optimized configuration on the seismic vulnerability and long-term performance of an isolated highway bridge. A typical three-span simply-supported highway bridge located in Vancouver, Canada, is considered in this study. The bridge is retrofitted with SMA cable restrainers as per previously proposed design guidelines. Fragility curves of the bridge retrofitted with SMA restrainers are assessed and compared with those of the original bridge structure and the bridges with elastic steel and CFRP cable restrainers. A total of 21 near-fault ground motions were used in the numerical simulations. Incremental dynamic analyses (IDAs) were performed to derive the fragility functions of the bridge. Two bridge components, including bridge piers and isolation bearings, are taken into account for generating the fragility curves of the bridge at both component and system levels. Finally, the long-term performance of the bridge is assessed by considering the corresponding economic impacts.

Previously, Li et al. (2018a) developed a displacement-based restrainer design guideline for isolated highway bridges. Then, the optimized configuration of SMA restrainers was numerically investigated by Wang et al. (2019b). This current paper focuses on probabilistic seismic risk assessment of the bridge retrofitted with the restrainers in an optimized configuration. The earlier papers proposed the design guideline and the optimized configuration. In order to close the above gaps, the current paper shows how the bridges with optimized restrainers perform under different earthquake scenarios. A probabilistic risk assessment was conducted to evaluate the seismic vulnerability and long-term performance of a typical three-span simply-supported highway bridge considering material uncertainties. The original contribution is to conduct a complete performance-based evaluation of the bridge equipped with optimized SMA restrainers in the light of performance-based earthquake engineering (PBEE). Another contribution is to provide a holistic image regarding the overall performance of such a novel bridge by assessing the life cycle economic losses of the bridge. This study is expected to provide some valuable insights and a holistic image of the long-term performance of such a structure for the decision making process.

2 Case study

2.1 Bridge description and modeling

A typical three-span simply-supported highway bridge isolated by LRBs is modeled and analyzed under seismic ground motions using finite element software OpenSees (McKenna

et al. 2000). The considered bridge type is a common bridge type. According to a detailed review conducted by the National Bridge Inventory (NBI), multi-span simply-supported highway bridges (MSSS) account for about 20% of the highway bridges and the most likely number of spans is three (Nielson and DesRoches 2007). As mentioned earlier, the response of base-isolated structures subjected to near-fault ground motions has been questioned in recent years (Dicleli 2007; Jónsson et al. 2010; Ismail and Casas 2014). It is mainly attributed to the distinct characteristics that make them different from far-field records, such as large long-period spectral components, long-duration pulse-like velocity waveform, and high peak ground velocities (Liao et al. 2004). In the latest studies, the same authors (Hedayati Dezfuli et al. 2017; Li et al. 2017a, b) have proved that the near-fault ground motions have a strong influence on the long-span or isolated bridges. In this regard, dynamic time history analyses are performed using 21 near-fault earthquake records having an epi-central distance smaller than 15 km. The detailed properties of these ground motions are listed in Table 1 (PEER 2018). Since the bridge is located in Vancouver city (western Canada) on Soil Class C (stiff soil), the ratio of PGA to PGV for these records is between 0.8 and 1.2 (Naumoski et al. 1988; Hedayati Dezfuli and Alam 2016). Considering PGA as the intensity measure (IM), the selected ground motions have PGA values ranging from 0.13 to 0.79 g.

The bridge consists of three-span reinforced concrete (RC) girders isolated by 30 rubber bearings installed between the girder and abutments, and the girder and pier caps. The

Table 1 Characteristics of near-fault ground motions

| No | Earthquake | Year | Magnitude (Richter) | Station component | Epicentral distance (km) | PGA (g) | PGV (cm/s) |
|----|-----------------|------|---------------------|-------------------|--------------------------|---------|------------|
| 1 | Chi-Chi | 1999 | 7.6 | TCU065-E | 2.5 | 0.79 | 115.0 |
| 2 | Chi-Chi | 1999 | 7.6 | TCU071-E | 5.8 | 0.53 | 52.3 |
| 3 | Chi-Chi | 1999 | 7.6 | TCU074-E | 13.5 | 0.38 | 44.9 |
| 4 | Chi-Chi | 1999 | 7.6 | TCU078-E | 8.2 | 0.45 | 40.2 |
| 5 | Chi-Chi | 1999 | 7.6 | TCU079-E | 11.0 | 0.59 | 70.5 |
| 6 | Chi-Chi | 1999 | 7.6 | TCU084-N | 11.5 | 0.43 | 48.1 |
| 7 | Imperial Valley | 1979 | 6.5 | CHI012 | 7.3 | 0.27 | 24.9 |
| 8 | Imperial Valley | 1979 | 6.5 | E08230 | 3.9 | 0.47 | 52.0 |
| 9 | Imperial Valley | 1979 | 6.5 | E11230 | 12.6 | 0.38 | 44.6 |
| 10 | Kobe | 1995 | 6.9 | KJM090 | 1.0 | 0.63 | 76.1 |
| 11 | Kobe | 1995 | 6.9 | NIS090 | 7.1 | 0.46 | 38.3 |
| 12 | Landers | 1992 | 7.3 | JOS000 | 11.0 | 0.27 | 27.6 |
| 13 | Loma Prieta | 1989 | 6.9 | BRN000 | 10.7 | 0.46 | 51.4 |
| 14 | Loma Prieta | 1989 | 6.9 | CLS090 | 3.9 | 0.48 | 47.6 |
| 15 | Loma Prieta | 1989 | 6.9 | G02000 | 11.1 | 0.37 | 36.8 |
| 16 | Loma Prieta | 1989 | 6.9 | SJTE225 | 14.7 | 0.28 | 28.2 |
| 17 | Northridge | 1994 | 6.7 | LOS070 | 12.4 | 0.47 | 41.1 |
| 18 | Northridge | 1994 | 6.7 | STC090 | 12.1 | 0.34 | 31.5 |
| 19 | Northridge | 1994 | 6.7 | PKC090 | 7.3 | 0.30 | 31.0 |
| 20 | Northridge | 1994 | 6.7 | RO3000 | 10.1 | 0.28 | 25.3 |
| 21 | Northridge | 1994 | 6.7 | GLE170 | 13.4 | 0.13 | 15.7 |

superstructure consists of 5 I-shape RC girders at each span and a 150 mm RC slab covered by 50 mm of asphalt layer. The concrete girders are supported on two RC multi-column bents. The detailed geometry of the bridge pier is illustrated in Fig. 1. The pier has a diameter of 900 mm and is reinforced with 18-M30 steel rebar (reinforcement ratio of 2.0%). D22 rebar is used as hoop reinforcement at a spacing of 300 mm. Three different types of restrainers (steel cable, CFRP cable, and SMA cable) are designed by the previously proposed design procedure (Li et al. 2018a) to limit the relative displacement between the pier and the bottom of the girder. The bridge is designed as per CHBDC (CSA S6-14 2014). Lead rubber bearings (LRBs) are designed to isolate the bridge according to the recommendation from AASHTO (2014) and Earthquake Engineering Handbook (Scawthorn and Chen 2003). All the bearings have the same plan area of 250 mm by 250 mm with identical total thicknesses of rubber layers (60 mm). The geometric details of the bridge, pier, and girders are shown in Fig. 1.

The superstructure, pier caps, and foundations are modeled using elastic beam-column elements so that these components remain elastic under earthquake excitations. The pounding effects of deck-deck and deck-abutment are represented by bilinear contact elements.

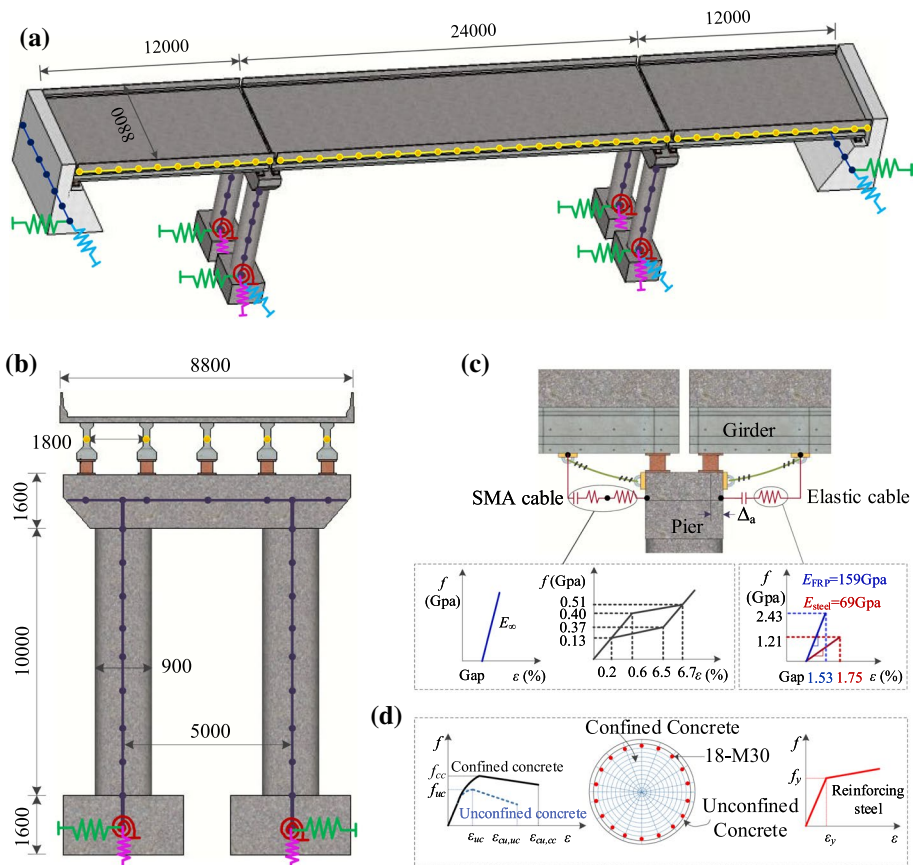


Fig. 1 Three-span simply-supported concrete-girder bridge (mm); **a** 3D configuration, **b** elevation view, **c** modeling of the restrainers and **d** pier section

Fiber-based nonlinear beam-column elements are used to describe the hysteretic behavior of the bridge bents. The confined, unconfined concrete and the longitudinal reinforcements are simulated using different stress–strain relationships (see Fig. 1d). The Chang and Mander (1994) uniaxial steel model simulated the behavior of the reinforcements (Grade 40). Concrete 01 was used to model the unconfined and confined concrete. The material properties of concrete and steel reinforcement are listed in Table 2. The behavior of the abutment is described by a bilinear demand model that accounts for expansion gaps incorporating a realistic value for the embankment fill response according to Caltrans (2013). The dynamic mechanism of the foundation is modeled by a series of zero-length linear rotational and translational spring elements. The stiffness values of the foundations are determined based on FHWA (2006). The bilinear kinematic model is ideally chosen to simulate the hysteretic behavior of LRBs. The initial stiffness, yield force, and post-yield hardening ratio of LRBs are 10.15 kN/mm, 15.1 kN, and 0.1, respectively.

The tension-only element is used to describe the behavior of the restrainers. Since the steel and CFRP cables are designed to remain elastic, an elastic-perfectly plastic gap model incorporating a uniaxial MinMax material is used to describe their elastic behavior. If the strain falls above the maximum threshold strain, the steel or CFRP cable is assumed to have failed and a value of 0.0 is returned for the stress. A combination of a tension-only gap element with high stiffness and a truss element with a flag-shaped constitutive model is combined to model the SMA cable restrainers. The material properties of restrainers are shown in Fig. 1c. Here, it should be mentioned that the stiffness and yield stress of the steel cable are different from those of the steel plate or reinforcing steel. According to the studies of DesRoches and Fenves (2000) and Saiidi et al. (2001), the modulus of elasticity of typical steel cables is 69 GPa. The cable restrainers are connected from the bottom of the

Table 2 Properties of the bridge

| Component | Material | Property | Value | Unit |
|--------------------|-------------------|---|-------|------|
| Pier | Concrete | Unconfined compressive strength, f_{uc} | 30 | MPa |
| | | Confined compressive strength, f_{cc} | 36.8 | MPa |
| | | Tensile strength | 0 | MPa |
| | | Strain at peak stress, ϵ_{uc} | 0.2 | % |
| | Reinforcing steel | Elastic modulus | 200 | GPa |
| | | Yield stress, f_y | 336 | MPa |
| | | Yield strain, ϵ_y | 0.17 | % |
| | | Strain hardening ratio | 0.5 | % |
| Restrainer (cable) | Steel | Elastic modulus, E_{steel} | 69 | GPa |
| | | Ultimate stress, $f_{u,steel}$ | 1210 | MPa |
| | FRP | Elastic modulus, E_{FRP} | 159 | GPa |
| | | Ultimate stress, $f_{u,FRP}$ | 2430 | MPa |
| | SMA | Modulus of elasticity | 66.7 | GPa |
| | | Austenite-to-martensite starting stress | 400 | MPa |
| | | Austenite-to-martensite finishing stress | 510 | MPa |
| | | Martensite-to-austenite starting stress | 370 | MPa |
| | | Martensite-to-austenite finishing stress | 130 | MPa |
| | | Stiffness, k_{abut} | 241 | MPa |
| Abutment | – | Passive pressure force, P_{bw} | 3968 | kN |

girders to the pier cap by using steel hooks (see Fig. 1c). More details can be found in the works of Li et al. (2018a) and Wang et al. (2019b).

2.2 Design of restrainers

The restrainers at abutment, end-span, and mid-span locations are designed independently according to the design procedure proposed by the same authors (Li et al. 2018a). A simplified model, i.e. a linearized two DOF analytical model, is used to design the restrainers as shown in Fig. 2b. A brief design procedure is provided as follows. More details with an example are available in Li et al. (2018a) and Wang et al. (2019b).

According to the geometric condition (see Fig. 2a), the design target displacement of the restrainer, Δ_d , can be calculated as

$$\Delta_d = \Delta_a - \Delta_s = L_{r1} \cos \theta_1 - L_{r0} \cos \theta_0 \tag{1}$$

where Δ_a is the allowable relative displacement between bridge girder and pier; Δ_s is the slack of the restrainer; L_{r0} , L_{r1} , θ_0 , and θ_1 are the lengths and the corresponding horizontal angles of the restrainer at initial and design target displacement conditions, respectively. L_{r1} and θ_1 can be determined as

$$\cos \theta_1 = \sqrt{1 - (\sin \theta_1)^2} = \sqrt{1 - \left(\frac{h_r}{L_{r1}}\right)^2} \tag{2}$$

$$L_{r1} = L_{r0} + \alpha \varepsilon_{max} L_{r0} \tag{3}$$

where h_r is the vertical distance between the two anchored ends of the restrainer; α is the normalized elongation ratio defined as the ratio of the axial deformation to the limit displacement of the restrainer; ε_{max} is the maximum applied strain of SMA. The design length of the restrainer, L_{r0} , can be calculated as Eq. 4 by substituting Eqs. 2 and 3 in Eq. 1.

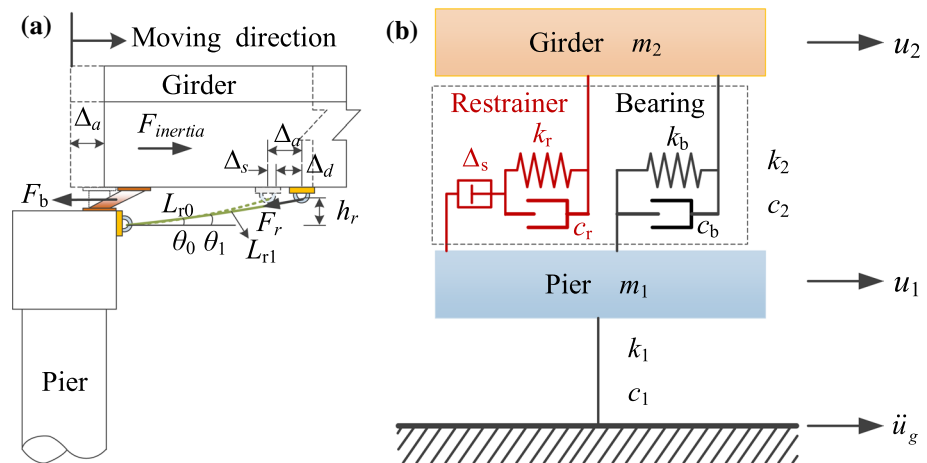


Fig. 2 Schematic view of a deformation and forces acting on the girders and b simplified model

$$L_{r0} = \frac{\Delta_d}{\sqrt{(1 + \alpha \epsilon_{\max})^2 - \sin^2 \theta_0} - \cos \theta_0} \tag{4}$$

According to the equilibrium of all forces in the horizontal direction (see Fig. 2a), the required force in the restrainer, F_r , can be derived as follows.

$$F_r = \frac{F_{inertia} - n_b F_b}{\cos \theta_1} = \frac{m_2 SA(T, \xi_0) - n_b F_b}{\sqrt{1 - \left(\frac{\sin \theta_0}{1 + \alpha \epsilon_{\max}}\right)^2}} \tag{5}$$

where $SA(T, \xi_0)$ is the design response spectra ordinate for period T and damping ratio ξ_0 ; $F_{inertia}$ is the inertia force of the girder; m_2 is the mass of the bridge girder; n_b is the number of isolation bearings at each pier or abutment location; F_b is the restoring force of the bearing at allowable displacement, Δ_a . Here, Δ_a can be determined by the designers according to several governing factors, such as the available seat width, initial gap between girders, limitation of the lateral design displacement, and the maximum shear strain of isolation bearings.

After obtaining the required strength of restrainers, the corresponding area can be calculated as follows.

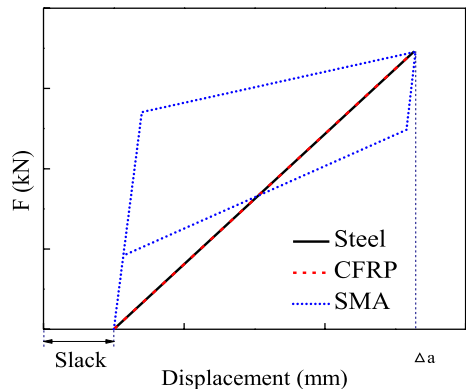
$$A_r = \frac{F_r}{f_a} \tag{6}$$

In which f_a represents the stress of the restrainer at allowable displacement, Δ_a .

In this study, the same value of Δ_a is used to design the restrainers. While using different types of restrainers, they are considered to have the same effective stiffness in the design procedure following the works of Andrawes and DesRoches (2007b) and Li et al. (2018a) (see Fig. 3).

Wang et al. (2019b) optimized the design parameters of the restrainers using fractional factorial design method. The optimized value of α and θ_0 are set as 1.0 and 0, respectively. Here, the restrainers at abutment location are designed based on a single DOF system. When designing the restrainers at endspan locations, the effects of abutment should be considered. In the design, the allowable displacement, Δ_a , and the slack in restrainers, Δ_s , are assumed as 150 mm and 25 mm, respectively. The material

Fig. 3 Mechanical properties of steel, CFRP, and SMA cables



properties of steel, CFRP, and SMA cable are illustrated in Fig. 1c. The designed parameters of the restrainers at different locations are listed in Table 3.

3 Methodology of seismic fragility and life-cycle loss assessment

3.1 Seismic vulnerability methodology

The probabilistic seismic demand model (PSDM) is employed to derive the analytical fragility curves in this study. The scaling approach is utilized to develop PSDM. The correlation between the engineering demand parameters (EDPs) and the corresponding intensity measures (IMs) is established by using the regression analysis in PSDM. It is assumed that the EDP follows a lognormal probability distribution (Song and Ellingwood 1999).

$$\ln(EDP) = \ln(a) + b \ln(IM) \tag{7}$$

where a and b are the regression coefficients that can be determined from a regression analysis of the response obtained from incremental dynamic analyses (IDAs).

Given the seismic demand and capacity, the fragility of each bridge component at a selected damage state, DS, can be calculated as follows.

$$P[DS|IM] = \Phi \left[\frac{\ln(IM) - \lambda}{\xi} \right] \tag{8}$$

where $\Phi(\cdot)$ is the cumulative distribution function of the standard normal distribution; λ and ξ are the median and the standard deviation of the IM , respectively.

$$\lambda = \frac{\ln(S_c) - \ln(a)}{b} \tag{9}$$

$$\xi = \frac{\sqrt{\beta_{D|IM}^2 + \beta_c^2}}{b} \tag{10}$$

where S_c and β_c are the median estimate and the logarithmic standard deviation of the capacity, respectively; $\beta_{D|IM}$ is the standard deviation of the demand that can be calculated as follows.

Table 3 Designed parameters for restrainers

| Restrainer | Allowable Δ_a (mm) | Slack Δ_s (mm) | Length L_r (m) | Area, A_r (mm ²) | | |
|------------|---------------------------|-----------------------|------------------|--------------------------------|----------|----------|
| | | | | Abut. | End-span | Mid-span |
| Steel | 150 | 25 | 7.13 | 258 | 258 | 834 |
| CFRP | 150 | 25 | 8.18 | 129 | 129 | 415 |
| NiTi SMA | 150 | 25 | 1.87 | 608 | 608 | 1961 |

Table 4 Limit states of bridge components

| Bridge component | EDP | Limit states | | | | Reference |
|-------------------|----------|--------------|----------|-----------|----------|---------------------|
| | | Slight | Moderate | Extensive | Collapse | |
| Pier | μ_d | 1.00 | 1.20 | 1.76 | 4.76 | Hwang et al. (2001) |
| Isolation bearing | γ | 100% | 150% | 200% | 250% | Zhang et al. (2009) |

Table 5 Capacity models of bridge components

| Limit states | Displacement ductility | | Shear strain | | Down-time (days) |
|--------------|------------------------|-----------|--------------|-----------|------------------|
| | S_c | β_c | S_c | β_c | |
| | Slight | 1.00 | 0.73 | 100 | |
| Moderate | 1.20 | 0.61 | 150 | 0.55 | 30 |
| Extensive | 1.76 | 0.74 | 200 | 0.59 | 120 |
| Collapse | 4.76 | 0.77 | 250 | 0.65 | 400 |

$$\beta_{D|IM} = \sqrt{\frac{\sum_{i=1}^N [\ln(EDP_i) - \ln(aIM_i^b)]^2}{N - 2}} \tag{11}$$

where N is the total number of simulation cases.

For highway bridges, bridge piers and isolation bearings are the main vulnerable components considering their nonlinear behaviors under earthquake excitations (Hedayati Dezfuli and Alam 2016; Xie and Zhang 2016; Zheng and Dong 2018). In this study, four limit states (namely slight, moderate, extensive, and collapse) defined in terms of EDPs are the same as those used in loss assessment package HAZUS-MH (FEMA 2003). The damage states of bridge piers and isolation systems are quantitatively measured by displacement ductility, μ_d , and shear strain, γ , respectively. According to the available literature (Hedayati Dezfuli and Alam 2016; Hwang et al. 2001; Zhang et al. 2009), the limit states for each bridge component are listed in Table 4. The distribution parameters of limit states, median estimate (S_c), and lognormal standard deviation (β_c) are identified to describe capacity models for each bridge component. Some levels of uncertainty are considered in the definition of the median values (Hedayati Dezfuli and Alam 2016). The distribution parameters of capacities are provided in Table 5 based on the recommendations in the literature (Hwang et al. 2001; Nielson and DesRoches 2007; Ramanathan et al. 2010; Hedayati Dezfuli and Alam 2016).

The fragility of the bridge at the system level can be developed from the fragilities of bridge components using the first-order reliability theory according to Eq. 12 (Nielson and DesRoches 2007; Hedayati Dezfuli and Alam 2016). This equation can be used to calculate the lower and upper bounds of the system fragility function. The lower bound refers to the components with complete correlation, while the upper bound assumes no correlation among components. If the lower bound is used to evaluate the system fragility, the failure probability of the system will be underestimated. In this regard, the upper bound is utilized to conservatively assess the vulnerability of the system.

$$\max_{i=1}^n (P[F_i]) \leq P_s \leq 1 - \prod_{i=1}^n (1 - P[F_i]) \tag{12}$$

where $P[F_i]$ and P_s are the failure probabilities of the i th component and system, respectively; n is the number of the vulnerable components, and Π is the product of the operator.

3.2 Life-cycle loss assessment

The life cycle performance assessment of a structure is a very complex process. Different methods with several assumptions have been proposed to assess the loss assessment of a structure in the literature. In this study, a framework proposed by Dong et al. (2013) was used to evaluate the long-term loss of the bridge retrofitted with SMA restrainers. The efficiency of the framework in assessing the seismic risk of a bridge structure has been validated in the works of Dong et al. (2013), Dong and Frangopol (2015, 2016), Zheng et al. (2018) and Zheng and Dong (2018).

In order to investigate the life-cycle performance of the bridge, the performance and damage probability of the bridge under earthquake excitations should be identified. The performance-based assessment approach proposed by the PEER center is adopted to compare the long-term performance of the bridges retrofitted with and without restrainers. The flowchart of the long-term life-cycle loss analysis for the isolated highway bridges retrofitted with restrainers is indicated in Fig. 4. In the procedure, both direct and indirect consequences, such as repair loss, running cost, property loss, etc. are considered in the life cycle context. Following the work of Dong et al. (2013) and Zheng et al. (2018), the repair cost of a bridge is regarded as the direct loss. Given the unit cost associated with downtime (e.g. \$/day), the corresponding indirect loss in the downtime can be calculated. As shown in Fig. 4, the hazard scenarios should be identified first to assess the seismic loss. In this study, five different hazard levels are considered and the expected life-cycle loss with respect to all the seismic events is calculated. The five considered hazard events are 225 (Event 1), 475 (Event 2), 975 (Event 3), 2475 (Event 4), and 5000-year (Event 5) return periods seismic intensities. According to CHBDC (CSA S6-14 2014), 2% probability of exceedance in 50 years with a 2475-year return period is regarded as the design event (DE). Here, the hazard curve is identified according to the USGS national seismic hazard map (USGS 2017). The seismic intensities (e.g. PGA) under different seismic scenarios can be calculated based on the hazard curve. Given the location of the bridge, the PGA associated with the five hazard events can be calculated. In this study, the PGAs with a return period of 225, 475, 975, 2475 and 5000 years are 0.1805, 0.2706, 0.3888, 0.5472, and 0.7042 g, respectively.

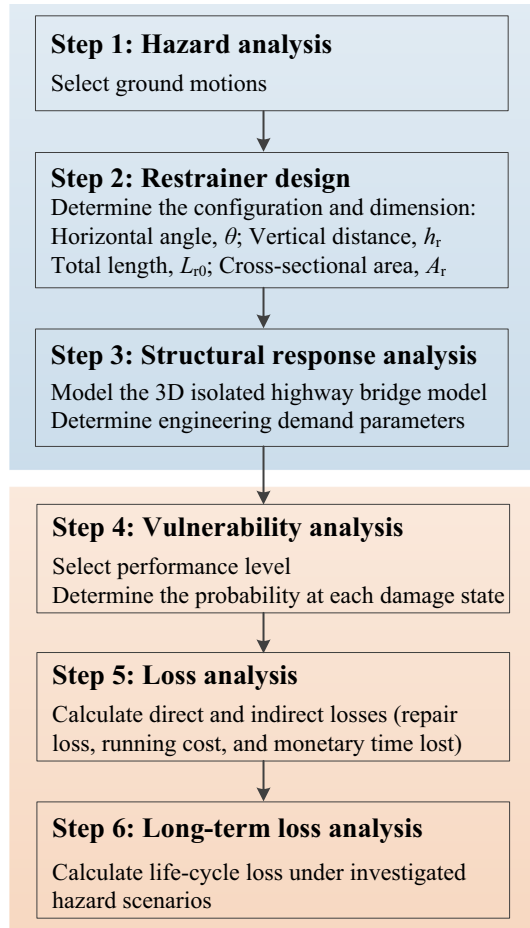
Under a given hazard event, the loss of the bridge, L_i , in economic metrics can be calculated as follows (Dong et al. 2013).

$$L_i = \sum_{i=1}^4 C_{DS,i} P_{DS,i|PGA} \tag{13}$$

where $C_{DS,i}$ denotes the consequences at a certain damage state, i , of the bridge; $P_{DS,i|PGA}$ denotes the conditional probability of a bridge at damage state i for a given PGA.

The repair cost at a certain damage state is assumed proportional to the rebuilding cost of the bridge and can be expressed as follows (Stein et al. 1999).

Fig. 4 Flowchart of the performance-based life-cycle analysis of isolated highway bridge retrofitted with restrainers under a seismic hazard



$$C_{REP,i} = R_{rcr} \cdot c_{reb} \cdot W \cdot L \tag{14}$$

where $C_{REP,i}$ is the repair cost of a bridge at damage state i ; c_{reb} is the rebuilding cost per square meter (unit: $\$/m^2$); W and L represent the width and length of the bridge (unit: m); R_{rcr} is the repair cost ratio at damage state i . Following the work of Mander (1999), the repair cost ratios at the slight, moderate, extensive, and collapse levels are 0.1, 0.3, 0.75, and 1.0, respectively.

Indirect costs considered in the current study include the running costs due to the bridge closure, C_{RUN} , and the monetary time lost for users and goods traveling, C_{TL} . Given a certain limit state i , these costs can be calculated as follows (Dong et al. 2013; Stein et al. 1999; Rackwitz 2002).

$$C_{RUN,i} = \left[c_{Run,car} \left(1 - \frac{T_0}{100} \right) + c_{Run,truck} \frac{T_0}{100} \right] \cdot D_l \cdot ADT \cdot d_i \tag{15}$$

$$C_{TL,i} = \left[c_{AW} o_{car} \left(1 - \frac{T_0}{100} \right) + (c_{ATC} o_{truck} + c_{goods}) \frac{T_0}{100} \right] \cdot \left[\frac{D_i \cdot ADT}{S} + ADTE \cdot \left(\frac{l}{S_D} - \frac{l}{S_0} \right) \right] d_i \tag{16}$$

where $c_{run,car}$, and $c_{run,truck}$ are the average costs for running cars and trucks per kilometer (unit: \$/km), respectively; T_0 is the ratio of the average daily truck traffic; D_i is the detour distance (unit: km); ADT is the average daily traffic to detour; $ADTE$ is the average daily traffic remaining on the damaged link; d_i is the duration of the detour listed in Table 5 (unit: day) (Padgett et al. 2009; Dong et al. 2013); c_{AW} and c_{ATC} are the average wages for car and truck drivers per hour (unit: \$/h), respectively; o_{car} and o_{truck} are the average vehicle occupancies for cars and trucks, respectively; c_{goods} is the time value of the goods transported in a cargo (unit: \$/h); S represents the average detour speed (unit: km/h); l is the route segment containing the bridge (unit: km); S_0 and S_D represent the average speed on the intact link and damaged link (unit: km/h), respectively.

By substituting Eqs. 14–16 in Eq. 13, the annual loss under the selected hazard can be determined. Then, the total loss of the bridge during the investigated time interval $(0, t_{int})$ can be calculated. Following the work of Dong and Frangopol (2016), the occurrence of an earthquake is assumed as a Poisson process. The total life-cycle hazard loss, LCL , can be determined as follows.

$$LCL_i(t_{int}) = \sum_{k=1}^{N(t_{int})} L_i(t_k) \cdot e^{-\tau t_k} \tag{17}$$

where $N(t_{int})$ denotes the number of earthquakes that occur during the time interval; $L_i(t_k)$ denotes the annual hazard loss at time t_k ; and τ denotes the monetary discount rate. The total expected lifetime failure loss of the bridge, $E[LCL(t_{int})]$, during the time interval, t_{int} , can be expressed as follows (Zheng et al. 2018).

$$E[LCL_i(t_{int})] = \frac{\lambda_f \cdot E(L_i)}{\tau} \cdot (1 - e^{-\tau t_{int}}) \tag{18}$$

where λ_f denotes the mean rate of the Poisson model; $E(L_i)$ is the expected annual hazard loss.

Following the relevant literature, the indirect loss assessment is based on a wide range of parameters. The reasonable value of each parameter plays an important role in the accuracy of results. Many factors may affect the values of the considered parameters, such as change of traffic flow over the bridge with time, the possibility of partially opening the bridge for traffic flow, wage or compensation level at the local economic level, the variation of link length, etc. It is clear that many parameters are dynamic and depend on the time, local economic level, repair strategy (the downtime, traffic control, selection of a detour), etc. It is hard to accurately evaluate the indirect loss. Hence, the values of these parameters used in this study are determined according to the relevant literature or seismic guidelines. However, given more information from the local transport agency, an accurate result can be easily obtained and updated. Besides, since it is not easy to know the number of casualties, the life loss cost is not considered in this study.

4 Fragility analysis of the isolated MSSS

As mentioned earlier, two critical components of the isolated MSSS, i.e. bridge pier and isolation bearing, which have major contributions to the system fragility, are considered in vulnerability analysis. Two engineering demand parameters are estimated, namely displacement ductility of bridge pier and shear strain of isolation bearing (Hedayati Dezfuli and Alam 2016).

4.1 Probabilistic seismic demand models (PSDM)

Prior to establishing the PSDM, the main uncertainties in modeling a bridge, i.e. material uncertainties, are considered to generate the bridge samples (Hwang et al. 2001). It is assumed that the concrete compressive strength and the yielding strength of reinforcing steel satisfy a normal distribution and lognormal distribution, respectively. The mean values of the compressive strength and the coefficient of variation (COV) are 30 MPa and 0.2, respectively. The yielding strength of reinforcement has a mean value of 336 MPa and the COV is 0.11. The Latin hypercube sampling (LHS) approach is used to generate 10 random bridge samples. As mentioned earlier, three-span simply supported highway bridges are a typical bridge type. The bridge type and the number of bridge spans are not considered as uncertainty parameters. Besides, the geometry of the bridge, mechanical uncertainties of the restrainers, etc. are not considered so that the design of the restrainer and the analyses could be simplified.

Each ground motion is scaled to 8 intervals in IDA and more than 1600 data sets are generated for the regression analysis. Thus, sufficient damage data corresponding to different intensity levels can be generated in PSDM. Displacement ductility, μ_d , of the bridge pier is defined as the ratio of the ultimate displacement, Δ_u , to the yield displacement, Δ_y . In elastomeric isolators, shear strain, γ , is defined as the ratio of the lateral deformation, Δ , to the total thickness of rubber layers, t_r . The probabilistic seismic demand models for the bridge pier and the isolation bearing in the logarithmic form are listed in Table 6 when the bridge is retrofitted with three different restrainers. It can be seen that the EDP and IM are linearly correlated where the R^2 values are higher than 0.85.

Table 6 PSDM for engineering demand parameters

| EDP | Restrainer | Response | PSDM $\ln a + b \ln(\text{PGA})$ | $\beta_{\text{D PGA}}$ | R^2 |
|----------------------|------------|---------------------------|--------------------------------------|------------------------|-------|
| γ | Without | $\ln(\gamma)$ | $\ln(204.9) + (0.90)\ln(\text{PGA})$ | 0.224 | 0.89 |
| | CFRP | $\ln(\gamma)$ | $\ln(162.5) + (0.82)\ln(\text{PGA})$ | 0.220 | 0.88 |
| | Steel | $\ln(\gamma)$ | $\ln(164.5) + (0.82)\ln(\text{PGA})$ | 0.216 | 0.89 |
| | SMA | $\ln(\gamma)$ | $\ln(116.9) + (0.64)\ln(\text{PGA})$ | 0.199 | 0.85 |
| μ_d | Without | $\ln(\mu_d)$ | $\ln(1.13) + (1.55)\ln(\text{PGA})$ | 0.421 | 0.90 |
| | CFRP | $\ln(\mu_d)$ | $\ln(1.28) + (1.54)\ln(\text{PGA})$ | 0.435 | 0.89 |
| | Steel | $\ln(\mu_d)$ | $\ln(1.32) + (1.56)\ln(\text{PGA})$ | 0.439 | 0.89 |
| | SMA | $\ln(\mu_d)$ | $\ln(1.32) + (1.42)\ln(\text{PGA})$ | 0.389 | 0.90 |
| Δ_{rd} | Without | $\ln(\Delta_{\text{rd}})$ | $\ln(143.4) + (0.90)\ln(\text{PGA})$ | 0.224 | 0.89 |
| | CFRP | $\ln(\Delta_{\text{rd}})$ | $\ln(113.6) + (0.82)\ln(\text{PGA})$ | 0.220 | 0.88 |
| | Steel | $\ln(\Delta_{\text{rd}})$ | $\ln(115.2) + (0.82)\ln(\text{PGA})$ | 0.216 | 0.89 |
| | SMA | $\ln(\Delta_{\text{rd}})$ | $\ln(81.8) + (0.64)\ln(\text{PGA})$ | 0.199 | 0.85 |

4.2 Component fragility curves

The fragility curves for the pier and bearing of the bridge retrofitted with different types of restrainers can be calculated according to Eq. 8. The median, λ , and the standard deviation, ξ , of PGA are quantified at each damage state using Eqs. 9 and 10, respectively (see Table 7). Then, the cumulative distribution functions can be calculated for each component at each damage level.

Figure 5 depicts the fragility curves of bearing at each damage state when different types of restrainers are utilized to retrofit the bridge. Results show that after retrofitting the bridge, the vulnerability of the isolation system noticeably decreases. The bearing in the case of SMA restrainers is less vulnerable compared to the unretrofitted bridge and the bridges with elastic restrainers at each damage state. The failure probabilities of the bridges with CFRP and steel restrainers are almost the same and lie in between those of the bridges with SMA restrainers and the unretrofitted bridge. The phenomenon can be explained by the following reasons. Compared to elastic restrainers, SMA restrainers can dissipate a large amount of earthquake energy and as a result, decrease the seismic responses of the bridge. Another point is that different types of restrainers have the same effective stiffness in the design procedure following the works of Andrawes and DesRoches (2007b) and Li et al. (2018a) (see Fig. 3). According to the design method, the restrainers can reach the same level of force at their design strain levels. The real stiffness of SMA restrainers during earthquakes is higher than that of the elastic restrainer. A sensitivity analysis has been conducted to evaluate the effect of the stiffness on the seismic performance of the restrainer in the latest work by Wang et al. (2019b). In this study, the optimized effective stiffness is used to design the restrainer. More details have been available in the works of Andrawes and DesRoches (2007b), Li et al. (2018a) and Wang et al. (2019b).

To be more specific, PGA with a value of 0.55 g, i.e. the design event considered in CHBDC (CSA S6-14 2014) (Event 4), is selected and failure probabilities at each damage state are listed in Table 8 for different types of restrainers. According to Table 8, at moderate limit state, CFRP, steel, and SMA restrainers can reduce the damage probabilities of bearing by 57.9%, 55.1%, and 88.4%, respectively. At the extensive limit state, the restrainers can reduce the damage probabilities of bearing by 71.8%, 69.2%, and 93.1%, respectively. Note that although the residual deformation of bridge bearings or decks is not the focus of this study, the authors find from the IDA that compared to steel and CFRP

Table 7 Mean and standard deviation of fragility functions

| Components | Restrainer | Slight | | Moderate | | Extensive | | Collapse | |
|-------------|------------|-----------|-------|-----------|-------|-----------|-------|-----------|-------|
| | | λ | ξ | λ | ξ | λ | ξ | λ | ξ |
| Bearing | Without | -0.80 | 0.66 | -0.35 | 0.66 | -0.03 | 0.70 | 0.22 | 0.77 |
| | CFRP | -0.59 | 0.72 | -0.10 | 0.72 | 0.25 | 0.76 | 0.52 | 0.83 |
| | Steel | -0.61 | 0.72 | -0.11 | 0.72 | 0.24 | 0.76 | 0.51 | 0.83 |
| | SMA | -0.25 | 0.92 | 0.39 | 0.92 | 0.85 | 0.98 | 1.20 | 1.07 |
| Bridge pier | Without | -0.08 | 0.55 | 0.09 | 0.48 | 0.29 | 0.55 | 0.93 | 0.57 |
| | CFRP | -0.16 | 0.55 | 0.01 | 0.49 | 0.21 | 0.56 | 0.86 | 0.58 |
| | Steel | -0.18 | 0.55 | -0.01 | 0.48 | 0.19 | 0.55 | 0.82 | 0.57 |
| | SMA | -0.20 | 0.59 | -0.01 | 0.52 | 0.21 | 0.60 | 0.91 | 0.62 |

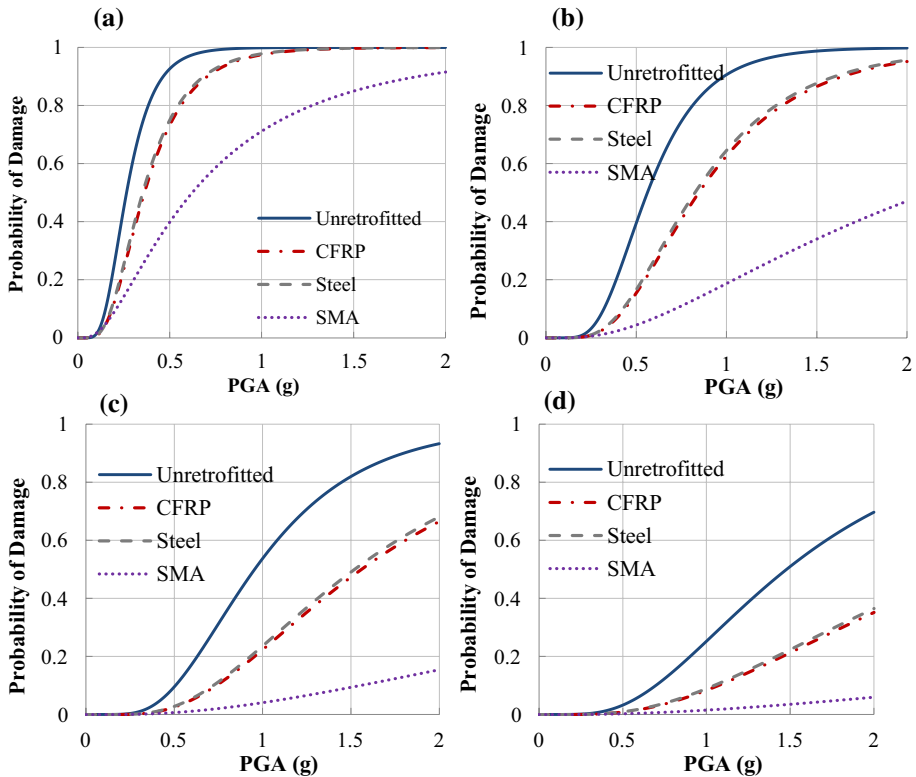


Fig. 5 Fragility curves of isolation bearing at **a** slight, **b** moderate, **c** extensive, and **d** collapse damage state

Table 8 Damage probabilities of bearing with different restrainers at 0.55 g PGA

| Restrainer | Slight | | Moderate | | Extensive | | Collapse | |
|------------|----------|--------------|----------|--------------|-----------|--------------|----------|--------------|
| | <i>P</i> | Δ (%) | <i>P</i> | Δ (%) | <i>P</i> | Δ (%) | <i>P</i> | Δ (%) |
| Without | 0.952 | – | 0.482 | – | 0.132 | – | 0.046 | – |
| CFRP | 0.789 | –17.1 | 0.206 | –57.9 | 0.039 | –71.8 | 0.012 | –72.8 |
| Steel | 0.804 | –15.6 | 0.221 | –55.1 | 0.042 | –69.2 | 0.014 | –70.2 |
| SMA | 0.442 | –53.6 | 0.069 | –88.4 | 0.014 | –93.1 | 0.004 | –92.0 |

P is the damage probability; Δ is the relative difference between damage probabilities of the bearing without restrainer and with two other types of restrainers

restrainers, SMA restrainers with a high re-centering capacity can significantly decrease the residual deformation of the bearings or the decks (more than 50%). For example, Fig. 6 shows the deformation of the bearings at the midspan location under the two most devastating earthquakes. As shown, the residual deformations of the bearings for the bridges retrofitted with steel and CFRP restrainers are 15.6 mm and 15.9 mm, respectively, under the Loma Prieta (BRN000) earthquake. After retrofitting the bridge with SMA restrainers, the corresponding value decreases to 6.9 mm under the same earthquake. In general, the

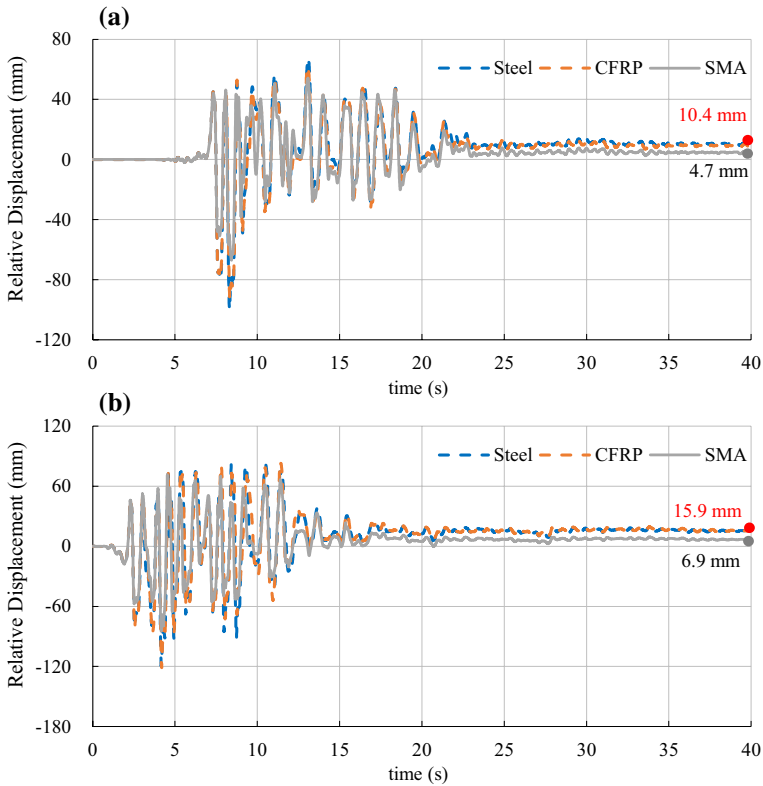


Fig. 6 Time history of the deformation of the bearings at the midspan location under Imperial Valley (E11230) and Loma Prieta (BRN000) earthquakes

average residual deformation of the bearings at the midspan location is calculated for the retrofitted bridges. Compared to steel and CFRP restrainers, SMA restrainers could reduce the residual deformation of the bearings by 51.4% and 53.2%, respectively.

Figure 7 illustrates the fragility curves of the bridge pier at each damage state. As observed in Fig. 7, at lower PGA, all the four bridges show small vulnerability at each limit state. However, at higher PGA, the use of restrainers in retrofitting the bridge can increase the damage probability of the pier as a result of the increased stiffness of the system. However, under Event 4 (design event) and Event 5 (maximum considered event), the damage probability of the bridge pier is less than 10% at the moderate, extensive, and collapse limit state. The restrainers do not considerably increase the fragilities of the bridge pier (see Table 9). Figure 7a shows that the retrofitted bridge pier may become more fragile at slight damage that could be repaired easily.

The elastic and superelastic restrainers cause similar damage probabilities in the bridge pier due to the same effective stiffness considered in the design procedure. However, compared to the elastic restrainers, the damage probabilities of the bridge pier with SMA restrainers increase at the slight, moderate, and extensive limit states for lower PGA values. For higher PGA values, the SMA retrofitted pier deem to have a better seismic performance due to the high energy dissipation capacity. It can be attributed to the fact that at low PGA values, the initial stiffness of SMA restrainers is higher than the

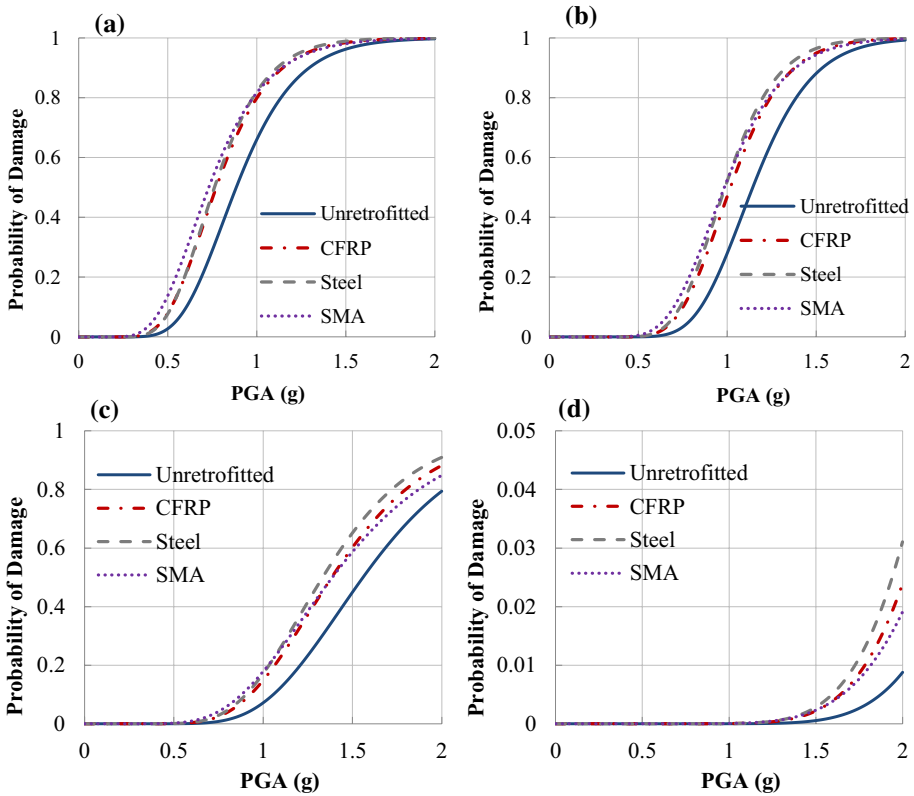


Fig. 7 Fragility curves of the bridge pier at **a** slight, **b** moderate, **c** extensive, and **d** collapse damage state

Table 9 Damage probabilities of bridge pier with different restrainers under Event 4 and Event 5

| Restrainer | Slight | | Moderate | | Extensive | | Collapse | |
|------------|---------------------|---------------------|---------------------|---------------------|---------------------|---------------------|---------------------|---------------------|
| | Event 4 (0.55 g) | Event 5 (0.70 g) | Event 4 (0.55 g) | Event 5 (0.70 g) | Event 4 (0.55 g) | Event 5 (0.70 g) | Event 4 (0.55 g) | Event 5 (0.70 g) |
| Without | 0.055 | 0.215 | 0.001 | 0.016 | 0.000 | 0.004 | 0.000 | 0.000 |
| CFRP | 0.124 | 0.358 | 0.005 | 0.057 | 0.002 | 0.014 | 0.000 | 0.000 |
| Steel | 0.136 | 0.387 | 0.006 | 0.068 | 0.002 | 0.017 | 0.000 | 0.000 |
| SMA | 0.208 | 0.452 | 0.014 | 0.100 | 0.005 | 0.027 | 0.000 | 0.000 |

elastic restrainers, which causes a higher seismic force demand in the pier. At high PGA values, the restrainers experience large amplitude deformations and SMA restrainers with a higher damping capacity compared to elastic restrainers, dissipate large seismic energy. According to the above analysis, both stiffness and energy dissipation capacity of restrainers have contributions to the fragility of the bridge component. Hence, the influence of the stiffness and energy dissipation capacity should be carefully considered in the design of restrainers.

4.3 System fragility curves

The upper bound of the first-order reliability theory in Eq. 12 is used to estimate the fragility of the bridge system. Using the upper bound can obtain a conservative evaluation of the failure probability of the system. Figure 8 shows the fragility curves of the isolated MSSS without restrainers and with CFRP, steel and SMA restrainers at four limit states. As can be seen, the bridge system without restrainers is more fragile than the retrofitted bridge at four limit states and PGA values ranging from 0 to 2.0 g. In the case of using CFRP and steel restrainers, the bridge systems are almost at the same level of vulnerability at four limit states, which means that elastic restrainers have nearly equal contributions to the fragility of the bridge system. Compared to elastic restrainers, SMA restrainers can effectively reduce the probability of damage to the bridge system. It is because the fragility reduction in the rubber bearing outweighs the increase of the fragility in the pier and as a result, the seismic vulnerability of the whole system decreases. It can be concluded that SMA restrainers perform more efficiently in improving the seismic performance of the bridge system.

In order to quantitatively compare the performance of three different restrainers, probabilities of damage of the isolated bridge are listed in Table 10 for five seismic events and

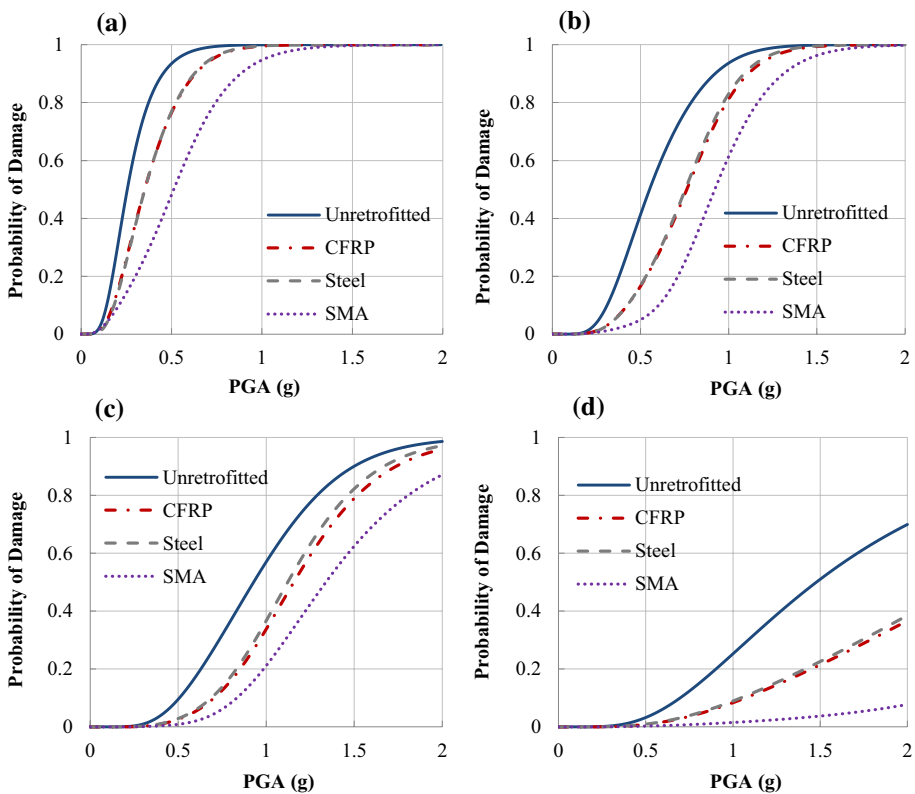


Fig. 8 Fragility curves of the bridge system retrofitted with different types of restrainers at **a** slight, **b** moderate, **c** extensive, and **d** collapse damage state

Table 10 Damage probabilities of the bridge system at each seismic event

| Event | Restrainer | Slight | | Moderate | | Extensive | | Collapse | |
|-------|------------|----------|--------------|----------|--------------|-----------|--------------|----------|--------------|
| | | <i>P</i> | Δ (%) | <i>P</i> | Δ (%) | <i>P</i> | Δ (%) | <i>P</i> | Δ (%) |
| E1 | Without | 0.188 | – | 0.005 | – | 0.000 | – | 0.000 | – |
| | CFRP | 0.088 | –53.4 | 0.001 | –70.2 | 0.000 | – | 0.000 | – |
| | Steel | 0.095 | –49.3 | 0.002 | –65.9 | 0.000 | – | 0.000 | – |
| | SMA | 0.072 | –61.7 | 0.001 | –68.4 | 0.000 | – | 0.000 | – |
| E2 | Without | 0.517 | – | 0.047 | – | 0.005 | – | 0.002 | – |
| | CFRP | 0.284 | –45.1 | 0.014 | –71.1 | 0.001 | –74.5 | 0.001 | –70.9 |
| | Steel | 0.301 | –41.8 | 0.015 | –67.7 | 0.002 | –71.1 | 0.001 | –67.2 |
| | SMA | 0.164 | –68.2 | 0.008 | –83.9 | 0.001 | –81.6 | 0.000 | –74.3 |
| E3 | Without | 0.795 | – | 0.186 | – | 0.031 | – | 0.010 | – |
| | CFRP | 0.539 | –32.2 | 0.061 | –67.3 | 0.008 | –74.7 | 0.003 | –73.0 |
| | Steel | 0.560 | –29.6 | 0.067 | –64.2 | 0.009 | –71.9 | 0.003 | –70.1 |
| | SMA | 0.302 | –62.0 | 0.022 | –88.4 | 0.003 | –89.8 | 0.001 | –87.0 |
| E4 | Without | 0.955 | – | 0.482 | – | 0.132 | – | 0.046 | – |
| | CFRP | 0.815 | –14.6 | 0.206 | –57.2 | 0.039 | –70.7 | 0.012 | –72.8 |
| | Steel | 0.831 | –13.0 | 0.221 | –54.2 | 0.042 | –68.0 | 0.014 | –70.2 |
| | SMA | 0.558 | –41.6 | 0.069 | –85.6 | 0.014 | –89.7 | 0.004 | –92.0 |
| E5 | Without | 0.990 | – | 0.698 | – | 0.268 | – | 0.101 | – |
| | CFRP | 0.934 | –5.6 | 0.394 | –43.6 | 0.098 | –63.3 | 0.029 | –71.2 |
| | Steel | 0.943 | –4.7 | 0.418 | –40.1 | 0.107 | –60.1 | 0.031 | –68.9 |
| | SMA | 0.756 | –23.6 | 0.186 | –73.3 | 0.044 | –83.6 | 0.007 | –93.4 |

four limit states. For Event 1 (225 year return period), both the retrofitted and unretrofitted bridges have very low damage probabilities at all limit states. For Event 2~5, the fragility of the retrofitted bridges presents a noticeable reduction at each limit state compared to the unretrofitted bridge. At the design event (Event 4), the damage probabilities of the unretrofitted bridge at slight, moderate, extensive, and collapse damage states are 0.980, 0.482, 0.132, and 0.046, respectively. When SMA restrainers are used, the probabilities of the bridge significantly reduce to 0.543, 0.069, 0.014, and 0.004, respectively. The bridges with CFRP and steel cables have similar and intermediate vulnerability compared to the unretrofitted bridge and the bridge with SMA restrainers. A similar phenomenon can be observed at other seismic events. Another important finding is that the SMA restrainers can effectively prevent the considered bridge from moderate and collapse damages under the maximum considered seismic event (5000-year return period). The probabilities of the bridge experiencing the extensive and collapse damages are only 4.4% and 0.7%, respectively.

4.4 Probability of unseating

The relative displacement between the girder and pier, Δ_{rd} , is considered as the *EDP* to evaluate the probability of unseating. In this study, the maximum relative displacement at the midspan location is considered to develop the fragility functions. Following the works of Li et al. (2018a), the seat width of the pier ($L_{sw}=400$ mm) is considered as the limit

value for the unseating of the bridge spans, i.e. collapse damage state. The corresponding limit values at slight, moderate, and extensive damage states are set as $0.25L_{sw}$, $0.50L_{sw}$, and $0.75L_{sw}$, respectively (Li et al. 2018a). Then, the PSDMs of Δ_{rd} can be derived and listed in Table 6. After calculating the PSDMs, the fragility curves at each damage state can be determined. Figure 9 illustrates the fragility curves of the bridge experiencing unseating of bridge spans.

It can be observed from Fig. 9 that the probabilities of the bridge at the four different damage states can be noticeably reduced by the use of the restrainers. Compared to the elastic restrainers, the superelastic SMA restrainers can significantly decrease the unseating probabilities of the bridge at each damage state. Another finding is that the bridges have a very low probability to experience the unseating of bridge spans (i.e. collapse damage) during the earthquakes. For example, at a PGA of 2.0 g, the unseating probabilities of the unretrofitted bridge and the bridges retrofitted with CFRP, steel, and SMA cables at collapse damage state are 2.5%, 0.43%, 0.47%, and 0.04%, respectively.

Here, it should be mentioned that the damage probabilities of the isolation bearings are used in the life cycle assessment without considering the probabilities of unseating due to the following reason. Since the limit values of Δ_{rd} at the slight, moderate, and extensive damage states are lower than L_{sw} , the economic loss of the bridge will be zero at these three damage states as there is no unseating in an actual situation. Also, the probabilities of observing a collapse damage state for the four bridges are very low ($< 2.5\%$). Hence, the loss induced by the unseating will be negligible. In this regard, the effects of unseating on the long-term loss of the bridges will not be considered in the following sections.

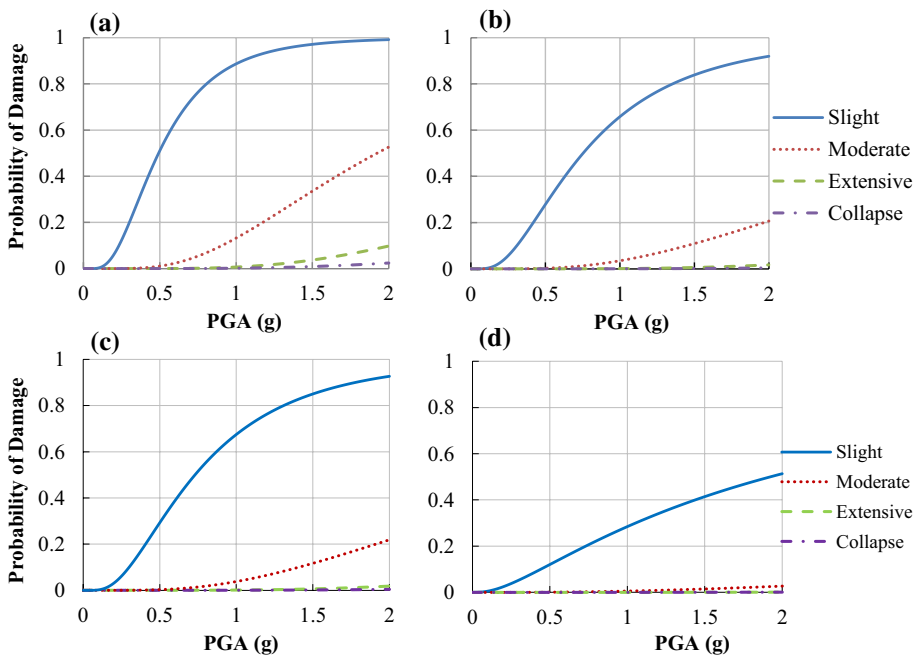


Fig. 9 Fragility curves of unseating of bridge spans for **a** the unretrofitted bridge and the bridge retrofitted with **b** CFRP cables, **c** steel cables, and **d** SMA cables

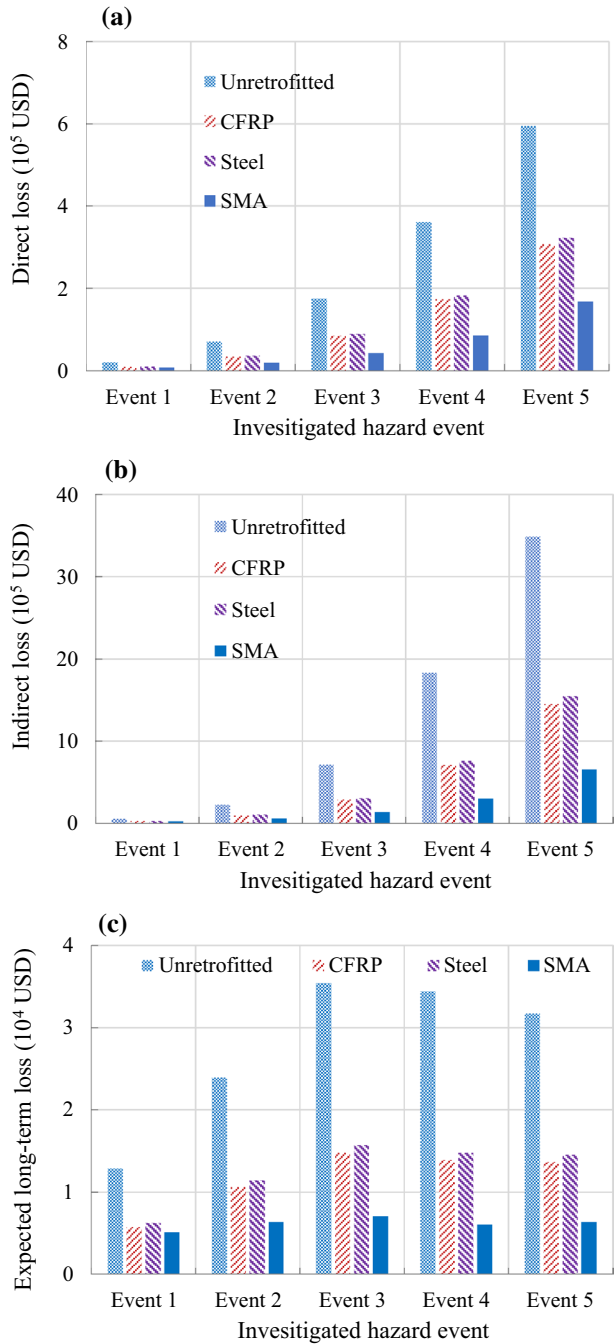
5 Long-term loss assessment of the isolated MSSS bridge

In order to evaluate the long-term performance of the isolated MSSS, the annual loss of the bridge at a particular seismic scenario can be calculated using Eq. 13. Considering a given seismic event, the failure probability of the bridge at each damage state can be quantified according to the fragility curves of the bridge systems. Then, the costs of all considered consequences, i.e., the direct and indirect costs, can be calculated using Eqs. 14–16. The parameters used in these equations are presented in Table 11. The expected repair and indirect losses of the bridges with different types of restrainers under the investigated five hazard events are illustrated in Fig. 10a, b. As can be seen, the seismic losses increase with the increase of the seismic intensity. The bridge without restrainers would result in a larger repair and indirect loss. After using restrainers to retrofit the bridge, the seismic loss could be significantly reduced. Among three considered restrainers, elastic restrainers (CFRP and steel cables) cause almost the same seismic loss, and SMA cables can make the bridge experience less seismic loss. In the case of Event 1 and 2, both the retrofitted and unretrofitted bridges experience low seismic losses (both direct and indirect). For the design event considered in CHBDC (CSA S6-14 2014) (Event 4), compared to the unretrofitted bridge, the direct losses of the bridge retrofitted with CFRP, steel, and SMA restrainers decrease by 52.1%, 49.6%, and 76.6%, respectively. The CFRP, steel, and SMA restrainers cause about 61.1%, 58.6%, and 83.6% reduction in the indirect losses, respectively. Another finding is that the indirect loss is much larger than the direct repair loss with the increase of seismic intensity. For instance, the indirect losses of

Table 11 Parameters associated with consequences

| Parameters | Notation | Value | References |
|---|-----------------|--------|--|
| Average daily traffic | ADT | 19,750 | Dong and Frangopol (2015) |
| Average daily traffic on the damage link to average daily traffic | ADTE/ADT | 0.12 | Decò and Frangopol (2011) |
| Daily truck traffic ratio | T_0 | 13% | FHWA (2015) |
| Link length (km) | l | 6 | FHWA (2015) |
| Detour additional distance (km) | D_1 | 2 | FHWA (2015) |
| Vehicle occupancies for cars | o_{car} | 1.5 | Stein et al. (1999) Dong and Frangopol (2016) |
| Vehicle occupancies for trucks | o_{truck} | 1.05 | Stein et al. (1999) Dong and Frangopol (2016) |
| Wage for car drivers (\$/h) | c_{AW} | 11.91 | Stein et al. (1999) Dong and Frangopol (2016) |
| Compensation for truck drivers (\$/h) | c_{ATC} | 29.87 | Stein et al. (1999) Dong and Frangopol (2016) |
| Operating costs for cars (\$/km) | $c_{Run,car}$ | 0.4 | Stein et al. (1999) Dong and Frangopol (2016) |
| Operating costs for trucks (\$/km) | $c_{Run,truck}$ | 0.57 | Stein et al. (1999) Dong and Frangopol (2016) |
| Rebuilding costs (\$/m ²) | c_{reb} | 2306 | Mander (1999) |
| Detour speed (km/h) | S | 50 | Dong and Frangopol (2016) |
| Link speed (km/h) | S_0 | 80 | Dong and Frangopol (2016) |
| Time value of a cargo (\$/h) | c_{goods} | 4 | Decò and Frangopol (2011) |
| Monetary discount rate | τ | 0.035 | Zheng et al. (2018) |

Fig. 10 Direct, indirect and long-term loss of the bridges under the five hazard events given $t_{int} = 75$ years and $\tau = 0.02$ **a** direct cost, **b** indirect cost, and **c** expected long-term loss



the unretrofitted bridge and the bridges with CFRP, steel, and SMA restrainers increase by 407%, 311%, 316%, and 256%, respectively, compared to the direct losses. In this regard, the

indirect loss should be considered in performance-based engineering. Without considering the contribution of indirect loss, one could underestimate the seismic loss of the bridge system.

In order to quantitatively evaluate the life-cycle performance of bridge systems with or without restrainers, the expected total loss under a given time interval is calculated using Eq. 18. It is assumed that the time interval and the monetary discount rate are 75 years and 2%, respectively. Here, the time interval is chosen according to the design service life of a bridge (i.e. 75 years) specified in the CHBDC (CSA S6-14 2014) and AASHTO (2012). Following the work of Zheng and Dong (2018), the monetary discount usually ranges from 2 to 7%. The lower and higher discount rates are usually used by the public sector and private sector, respectively. In this regard, the lower discount rate is considered in the lifetime failure cost assessment.

The expected long-term losses of the bridges under the five events are illustrated in Fig. 10c. As can be observed, the long-term losses of both the retrofitted and unretrofitted bridges under Event 3 are larger than four other events. This is because both the occurrence probability and the hazard intensity of the hazard event have contributions to the expected long-term loss. Thus, the 975-year return period event (Event 3) chosen as the design event (DE) could be reasonable for the unretrofitted bridge considering its long-term seismic loss as evident in other design codes (Caltrans BDA 2013; AASHTO LRFD 2012; Chinese Guidelines for Seismic Design of Highway Bridges JTG/T BO2-01-2008; European 8 2005). Hence, the design event specified in CHBDC (CSA S6-14 2014) may underestimate the long-term seismic losses of the bridge for more frequently occurring earthquakes having lower return periods over its service life.

Compared to elastic restrainers, SMA restrainers are more economically benefit under strong seismic events with a low probability of occurrence. In the case of Event 3 with a 975-year return period, compared to the unretrofitted bridge, using CFRP, steel, and SMA restrainers can reduce the long-term seismic losses by 58.4%, 55.6%, and 80.1%, respectively. For the design event (Event 4), expected long-term loss of the bridge retrofitted with SMA restrainers is about 6036 USD, which is approximate 17.6% of that of the unretrofitted bridge. Here, it should be mentioned that although the seismic intensity of Event 4 is larger than the Event 3, the expected long-term loss of the former one is lower than that of the latter one. The reason is that the probability of occurrence of Event 3 is higher than that of Event 4 during the investigated time interval (see Figs. 10, 11). The relationship between the return period of the seismic event and expected long-term loss is illustrated in Fig. 11. As indicated, the bridge with SMA restrainers would result in the smallest long-term loss, given the return period of the seismic event is larger than 225 years (Event 1).

As mentioned earlier, a wide range of parameters has certain impacts on the long-term loss assessment. Here, the effects of two main parameters, i.e. the investigated time interval (t_{int}) and monetary discount rate (τ) on the total expected long-term loss are evaluated. As observed in Fig. 12, the expected loss increases as the time interval increases, while the expected loss presents a decrease trending with the increase of monetary discount rate. As t_{int} or τ increase, the slope of each curve decreases. Hence, in order to make the long-term loss more accurate and improve the level of prediction, the relevant factors should be carefully determined according to more accurate information.

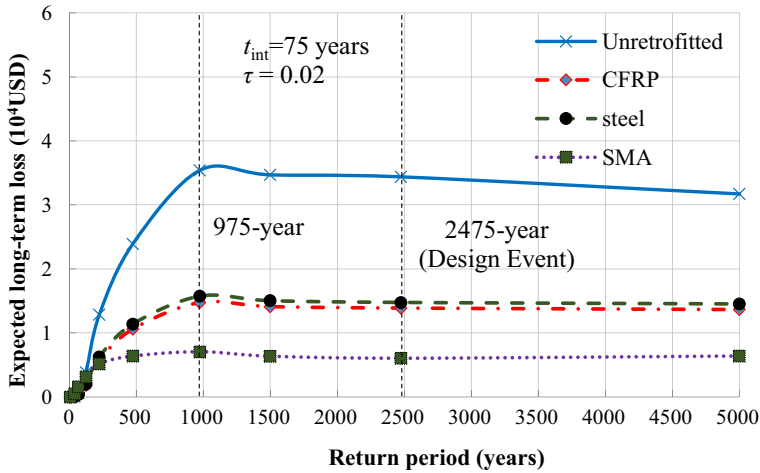


Fig. 11 Variations of the expected long-term loss with the return period of seismic events

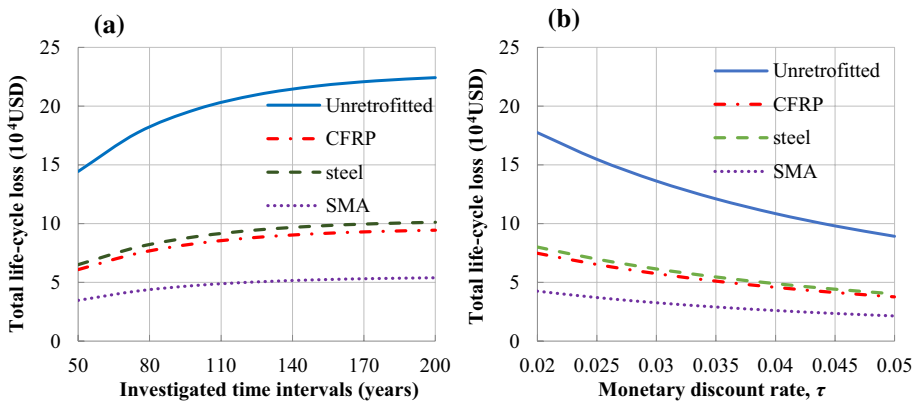


Fig. 12 Effect of a investigated time interval and b monetary discount rate on the expected long-term loss

6 Conclusions

The fragility and long-term performance of a typical multi-span simply-supported (MSSS) bridge retrofitted with optimized SMA restrainer were analytically evaluated and compared with the unretrofitted bridge and the bridges with elastic restrainers (i.e. steel and CFRP cable). A newly proposed design procedure was used to properly design the restrainers for the bridge. The optimized configuration of the restrainers was identified using a fractional factorial design method. Two critical vulnerable components (bridge pier and isolation bearing) were considered to develop the fragility curves of the bridge system. Then, life-cycle loss under five investigated hazard events was estimated considering the direct (repair cost) and indirect (running cost and monetary time lost) loss. This study is expected to provide directions to the decision-makers through life-cycle cost analysis towards the application of costly SMA restrainers in the seismic design process. The following conclusions can be drawn.

1. Restrainers increase the lateral stiffness of the bridge, and as a result, cause a lower deformation of bearings, but a higher seismic force demand in the bridge pier. When the considered bridge was retrofitted with elastic restrainers, i.e. CFRP and steel cables, the bridge components (bridge pier and isolation bearing) and the system reached almost the same level of vulnerability at four limit states.
2. Implementing superelastic SMA restrainers instead of elastic restrainers made the bearing less fragile; however, it caused the pier more fragile at low PGA values while reducing the damage probabilities at high PGA values. It could be attributed to the higher stiffness that increased the vulnerability at low PGAs whereas, increased energy dissipation capacity of SMA restrainer could reduce the vulnerability at high PGAs.
3. The use of restrainers in retrofitting the bridge could noticeably decrease the damage probability of the bridge system. Elastic restrainers like steel and CFRP cables with no energy dissipation capacity had almost the same contributions to the vulnerability of the system. Due to superior energy dissipation capacity, superelastic SMA restrainers could significantly reduce the failure probability of the bridge. The damage probabilities of the bridge with elastic restrainers lay in between those of the bridges with SMA restrainers and the unretrofitted bridge. Under DE and MCE, the probabilities of the bridge retrofitted with SMA restrainers experiencing the collapse damage are only 0.4% and 0.7%, respectively.
4. Since the largest expected long-term loss occurred in the 975-year return period event for the bridge without restrainers or with restrainers, the event with a 5% probability of exceedance in 50 years is reasonably chosen as the design event (DE) as recommended in several design codes. The design event specified in CHBDC (CSA S6-14 2014) (the 2475-year return period event) may underestimate the long-term seismic losses of the highway bridges considering its low probability of occurrence during its service life compared to the 975-year return period event.
5. After implementing the restrainers, the seismic loss of the bridge system could be reduced remarkably. The SMA restrainers would result in a larger benefit for the bridges located in seismic regions compared to the elastic restrainers. For example, the expected long-term loss of the bridge retrofitted with SMA restrainers under DE is approximate 17.6% of that with respect to the unretrofitted bridge.

The life cycle performance assessment of a structure is a very complex process. Generally, it can be quantified in terms of social, environmental, and economic metrics. In addition, since the long-term performance assessment is based on the fragility functions, a wide range of factors, such as type and geometry of the bridge, IMs, earthquake (far-field and near-fault), location, soil-structure interaction (SSI), should be considered to capture uncertainties and minimize errors. In this study, some assumptions were made to simplify the problem and the design of the restrainer. Hence, in order to improve the accuracy of the fragility and the level of prediction in the long-term performance, a further comprehensive study should be conducted to better understand the contributions of restrainers of a bridge system in the long run. The fragility functions and long-term performance assessment for the bridge system can be used for evaluating the potential seismic losses and aiding pre-event decision making according to proper retrofit strategies. Moreover, it can also be useful to help decision-makers make plans for post-earthquake.

Acknowledgements This study was financially supported by the Fundamental Research Funds for the Central Universities (Grant No. 2242019K40082), the National Natural Science Foundation of China (Grant No.

51908123), the Natural Science Foundation of Jiangsu Province (Grant No. BK20190370), and Natural Sciences and Engineering Research Council (NSERC) of Canada through Discovery Grant.


References

- AASHTO (2012) Guide specifications for LRFD bridge design specifications. LRFDUS-6, 6nd ed., Washington DC
- AASHTO (2014) Guide specifications for seismic isolation design, 4nd ed., Washington DC
- Alam MS, Bhuiyan MAR, Billah AHMM (2012) Seismic fragility assessment of SMA-bar restrained multi-span continuous highway bridge isolated by different laminated rubber bearings in medium to strong seismic risk zones. *B Earthq Eng* 10(6):1885–1909
- Andrawes B, DesRoches R (2005) Unseating prevention for multiple frame bridges using superelastic devices. *Smart Mater Struct* 14(3):S60
- Andrawes B, DesRoches R (2007a) Effect of ambient temperature on the hinge opening in bridges with shape memory alloy seismic restrainers. *Eng Struct* 29(9):2294–2301
- Andrawes B, DesRoches R (2007b) Comparison between shape memory alloy seismic restrainers and other bridge retrofit devices. *J Bridge Eng ASCE* 12(6):700–709
- Aryan H, Ghassemieh M (2015) Seismic enhancement of multi-span continuous bridges subjected to three-directional excitations. *Smart Mater Struct* 24(4):045030
- Bhuiyan MAR, Alam MS (2012) Seismic vulnerability assessment of a multi-span continuous highway bridge fitted with shape memory alloy bars and laminated rubber bearings. *Earthq Spectra* 28(4):1379–404
- Caltrans (2013) Seismic design criteria, Sacramento
- Canadian Standards Association (2014) CAN/CSA-S6-14—Canadian highway bridge design code. Canadian Standards Association, Rexdale
- CEN (2005) Eurocode 8: design of structures for earthquake resistance—part 3: seismic actions and geotechnical aspects. EN 1998-1, Brussels
- Chang GA, Mander JB (1994) Seismic energy based fatigue damage analysis of bridge columns: part I—evaluation of seismic capacity. National Center for Earthquake Engineering Research, Buffalo, p 222
- Chen LS (2012) Report on highways' damage in the Wenchuan earthquake. China Communications Press, Beijing
- Decò A, Frangopol DM (2011) Risk assessment of highway bridges under multiple hazards. *J Risk Res* 14(9):1057–1089
- DesRoche R, Delemont M (2002) Seismic retrofit of simply supported bridges using shape memory alloys. *Eng Struct* 24:325–332
- DesRoches R, Fenves GL (2000) Design of seismic cable hinge restrainers for bridges. *J Struct Eng ASCE* 126(4):500–509
- DesRoches R, Pfeifer T, Leon RT et al (2003) Full-scale tests of seismic cable restrainer retrofits for simply supported bridges. *J Bridge Eng* 8(4):191–198
- Dicleli M (2007) Supplemental elastic stiffness to reduce isolator displacements for seismic-isolated bridges in near-fault zones. *Eng Struct* 29(5):763–775
- Dong Y, Frangopol DM (2015) Risk and resilience assessment of bridges under mainshock and aftershocks incorporating uncertainties. *Eng Struct* 83:198–208
- Dong Y, Frangopol DM (2016) Probabilistic time-dependent multihazard life-cycle assessment and resilience of bridges considering climate change. *J Perform Constr Fac* 30(5):1–12
- Dong Y, Frangopol DM, Saydam D (2013) Time-variant sustainability assessment of seismically vulnerable bridges subjected to multiple hazards. *Earthq Eng Struct Dyn* 42(10):1451–1467
- FEMA (Federal Highway Administration) (2003) HAZUS-MH MR1: technical manual, vol. earthquake model. Federal Emergency Management Agency, Washington, DC
- FHWA (Federal Highway Administration) (2006) Seismic retrofitting manual for highway structures: part 1-bridges. U.S. Dept. of Transportation, Washington, DC
- FHWA (Federal Highway Administration) (2015) National bridge inventory (NBI) database. U.S. Dept. of Transportation, Washington, DC
- Guo A, Zhao Q, Li H (2012) Experimental study of a highway bridge with shape memory alloy restrainers focusing on the mitigation of unseating and pounding. *Earthq Eng Eng Vib* 11(2):195–204
- Hedayati Dezfuli F, Alam MS (2016) Seismic vulnerability assessment of a steel-girder highway bridge equipped with different SMA wire-based smart elastomeric isolators. *Smart Mater Struct* 25(7):075039

- Hedayati Dezfuli F, Li S, Alam MS et al (2017) Effect of constitutive models on the seismic response of an SMA-LRB isolated highway bridge. *Eng Struct* 148:113–125
- Hwang H, Liu JB, Chiu YH (2001) Seismic fragility analysis of highway bridges. MAEC Technical Report MAEC RR-4. Mid-America Earthquake. Center, University of Illinois, Urbana-Champaign
- Hwang JS, Wu JD, Pan T, Yang G (2002) A mathematical hysteretic model for elastomeric isolation bearings. *Earthq Eng Struct Dyn* 31:771–789
- Ismail M, Casas JR (2014) Novel isolation device for protection of cable-stayed bridges against near-fault earthquakes. *J Bridge Eng* 19(8):A4013002
- Joghataie A, Pahlavan Yali A (2015) Improved seismic response of multispan bridges retrofitted with compound restrainers. *Sci Iran* 22(4):1422–1434
- Joghataie A, Pahlavan Yali A (2017) Numerical assessment of new compound restrainer for seismic retrofit of bridges. *Struct Infrastruct Eng* 2017:1–20
- Johnson R, Padgett JE, Maragakis ME et al (2008) Large scale testing of Nitinol shape memory alloy devices for retrofitting of bridges. *Smart Mater Struct* 17(3):035018
- Jónsson MH, Bessason B, Hafþidason E (2010) Earthquake response of a base-isolated bridge subjected to strong near-fault ground motion. *Soil Dyn Earthq Eng* 30(6):447–455
- JTG/T B02–01–2008 (2008) Chinese guidelines for seismic design of highway bridges. People's Communications Press, Beijing
- Julian FDR, Hayashikawa T, Obata T (2007) Seismic performance of isolated curved steel viaducts equipped with deck unseating prevention cable restrainers. *J Constr Steel Res* 63(2):237–253
- Kawashima K, Takahashi Y, Ge H, Wu Z, Zhang J (2009) Reconnaissance report on damage of bridges in 2008 Wenchuan, China, earthquake. *J Earthq Eng* 13(7):965–996
- Li S, Zhang F, Wang JQ, Zhang J, Alam MS (2017a) Effects of near-fault motions and artificial pulse-type ground motions on super-span cable-stayed bridge systems. *J Bridge Eng ASCE* 22:04016128
- Li S, Zhang F, Wang JQ et al (2017b) Seismic responses of super-span cable-stayed bridges induced by ground motions in different sites relative to fault rupture considering soil-structure interaction. *Soil Dyn Earthq Eng* 101:295–310
- Li S, Hedayati Dezfuli F, Wang JQ, Alam MS (2018a) Displacement-based seismic design of steel, FRP and SMA cable restrainers for isolated simply supported bridges. *J Bridge Eng ASCE* 23(6):04018032
- Li S, Hedayati Dezfuli F, Wang JQ, Alam MS (2018b) Longitudinal seismic response control of long-span cable-stayed bridges using shape memory alloy wire-based lead rubber bearings under near-fault records. *J Intell Mater Syst Struct* 29(5):703–728
- Liao WI, Loh CH, Lee BH (2004) Comparison of dynamic response of isolated and non-isolated continuous girder bridges subjected to near-fault ground motions. *Eng Struct* 26(14):2173–2183
- Mander JB (1999) Fragility curve development for assessing the seismic vulnerability of highway bridges. Technical Report, University at Buffalo, State University of New York
- Markogiannaki O, Tegos I (2014) Seismic reliability of a reinforced concrete retrofitted bridge, safety, reliability, risk and life-cycle performance of structures and infrastructures. CRC Press, Boca Raton, pp 4229–4236
- McKenna F, Fenves GL, Scott MH (2000) Open system for earthquake engineering simulation (OpenSees). University of California, Berkeley. <http://opensees.berkeley.edu>. Accessed 26 June 2016
- Naeim F, Kelly J M (1999) Design of seismic isolated structures: from theory to practice. Wiley
- Naumoski N, Tso WK, Heidebrecht AC (1988) A selection of representative strong motion earthquake records having different A/V ratios. EERG Report 88-01, Earthquake Engineering
- Nielson BG (2005) Analytical fragility curves for highway bridges in moderate seismic zones. Doctoral dissertation, Georgia Institute of Technology, Atlanta
- Nielson BG, DesRoches R (2007) Seismic fragility methodology for highway bridges using a component level approach. *Earthq Eng Struct Dyn* 36(6):823–839
- Ozbulut OE, Hurllebaus S (2010) Optimal design of superelastic-friction base isolators for seismic protection of highway bridges against near-field earthquakes. *Earthq Eng Struct Dyn* 40(3):273–291
- Ozbulut OE, Hurllebaus S (2011) Seismic assessment of bridge structures isolated by a shape memory alloy/rubber-based isolation system. *Smart Mater Struct* 20:015003
- Padgett JE, DesRoches R (2008) Three-dimensional nonlinear seismic performance evaluation of retrofit measures for typical steel girder bridges. *Eng Struct* 30(7):1869–1878
- Padgett JE, Ghosh J, Dennemann K (2009) Sustainable infrastructure subjected to multiple threats. TCLEE 2009: lifeline earthquake engineering in a multi-hazard environment. ASCE, pp 703–713
- Padgett JE, DesRoches R, Ehlinger R (2010) Experimental response modification of a four span bridge retrofit with shape memory alloys. *Struct Control Health Monit* 17(6):694–708
- PEER (Pacific Earthquake Engineering Research Center) (2018) Strong motion database. <http://ngawest2.berkeley.edu/>. Accessed 12 Oct 2018

- Rackwitz R (2002) Optimization and risk acceptability based on the life quality index. *Struct Saf* 24(2–4):297–331
- Ramanathan K, DesRoches R, Padgett JE (2010) Analytical fragility curves for multi-span continuous steel girder bridges in moderate seismic zones Transportation Research Record 2202. Transportation Research Board, Washington, DC, pp 173–182
- Research Group, Department of Civil Engineering, McMaster University, Hamilton, ON, Canada
- Saiidi M, Maragakis E, Feng S (1996) Parameters in bridge restrainer design for seismic retrofit. *J Struct Eng ASCE* 121(1):61–68
- Saiidi M, Randall M, Maragakis E et al (2001) Seismic restrainer design methods for simply supported bridges. *J Bridge Eng ASCE* 6(5):307–315
- Saiidi MS, Johnson R, Maragakis EM (2006) Development, shake table testing, and design of FRP seismic restrainers. *J Bridge Eng ASCE* 11(4):499–506
- Scawthorn C, Chen WF (2003) Earthquake engineering handbook. CRC Press, Boca Rotan
- Schiff AJ (1995) Northridge earthquake, lifeline performance and postearthquake response. TCLEE monograph series. ASCE, Reston
- Shen J, Tsai MH, Chang KC, Lee GC (2004) Performance of a seismically isolated bridge under near-fault earthquake ground motions. *J Struct Eng ASCE* 130(6):861–868
- Shrestha B, He LX, Hao H et al (2018) Experimental study on relative displacement responses of bridge frames subjected to spatially varying ground motion and its mitigation using superelastic SMA restrainers. *Soil Dyn Earthq Eng* 109:76–88
- Siddiquee K, Alam M (2017) Highway bridge infrastructure in the province of British Columbia (BC), Canada. *Infrastructures* 2(2):7
- Song J, Ellingwood BR (1999) Seismic reliability of special moment steel frames with welded connections. *J Struct Eng ASCE* 125:372–384
- Stein SM, Young GK, Trent RE, Pearson DR (1999) Prioritizing scour vulnerable bridges using risk. *J Infrastruct Syst* 5(3):95–101
- USGS (2017) Unified hazard tool. <https://earthquake.usgs.gov/hazards/interactive/>. Accessed 10 Oct 2018
- Wang CL, Gao Y, Cheng X et al (2019a) Experimental investigation on H-section buckling-restrained braces with partially restrained flange. *Eng Struct* 199:109584
- Wang J, Li S, Dezfuli FH et al (2019b) Sensitivity analysis and multi-criteria optimization of SMA cable restrainers for longitudinal seismic protection of isolated simply supported highway bridges. *Eng Struct* 189:509–522
- Xiang N, Li J (2017) Experimental and numerical study on seismic sliding mechanism of laminated-rubber bearings. *Eng Struct* 141:159–174
- Xiang N, Alam MS, Li J (2018) Shake table studies of a highway bridge model by allowing the sliding of laminated-rubber bearings with and without restraining devices. *Eng Struct* 171:583–601
- Xie Y, Zhang J (2016) Optimal design of seismic protective devices for highway bridges using performance-based methodology and multiobjective genetic optimization. *J Bridge Eng ASCE* 22(3):04016129
- Zhang J, Huo Y (2009) Evaluating effectiveness and optimum design of isolation devices for highway bridges using the fragility function method. *Eng Struct* 31:1648–1660
- Zhang Y, Hu H, Zhu S (2009) Seismic performance of benchmark base-isolated bridges with superelastic Cu–Al–Be restraining damping device. *Struct Control Hlth* 16:668–685
- Zheng Y, Dong Y (2019) Performance-based assessment of bridges with steel-SMA reinforced piers in a life-cycle context by numerical approach. *B Earthq Eng* 17(3):1667–1688
- Zheng Y, Dong Y, Li Y (2018) Resilience and life-cycle performance of smart bridges with shape memory alloy (SMA)-cable-based bearings. *Constr Build Mater* 158:389–400

Affiliations

Shuai Li^{1,2} · Farshad Hedayati Dezfuli² · Jing-quan Wang¹ · M. Shahría Alam² 

Shuai Li
hmlishuai@163.com

Farshad Hedayati Dezfuli
farshad.hedayati@alumni.ubc.ca

¹ School of Civil Engineering, Southeast University, Nanjing 210096, Jiangsu, People's Republic of China

² School of Engineering, The University of British Columbia, Kelowna, BC V1V1V7, Canada